JOINT EUROPEAN TORUS JET

JET–P(93)11

F.B. Marcus, J. M. Adams, B. Balet, D.S. Bond,
S.W. Conroy, P.J.A. Howarth, O.N. Jarvis, M.J. Loughlin,
G.J. Sadler, P. Smeulders, N. Watkins

Neutron Emission Profile Measurements during the First Tritium Experiments at JET

Neutron Emission Profile Measurements during the First Tritium Experiments at JET

F.B. Marcus, J. M. Adams[1], B. Balet, D.S. Bond[1],
S.W. Conroy, P.J.A. Howarth[2], O.N. Jarvis, M.J. Loughlin,
G.J. Sadler, P. Smeulders, N. Watkins[1]

JET-Joint Undertaking, Culham Science Centre, OX14 3DB, Abingdon, UK

[1]AEA Industrial Technology, Harwell Laboratory, Oxon, OXll ORA, UK.
[2]University of Birmingham, Birmingham, B15 2TT, UK.

Preprint of a paper to be submitted for publication in Nuclear Fusion
February 1993

ABSTRACT

During a series of experiments with tritium (t) in deuterium (d) plasmas in the Joint European Torus (JET), the temporal evolution and the two-dimensional (2-D) spatial profiles of the 2.5 and 14MeV neutron emissivity from d-d and d-t fusion reactions were inferred from measurements with the JET neutron emission profile monitor. These experiments, involving triton production from d-d fusion, beam deposition and diffusion, d-t fusion, and tritium removed from wall tiles, were investigated in four plasma scenarios: (i) In high performance deuterium plasmas with deuterium neutral beam injection, the 14MeV neutron emissivity due to triton burnup was observed. (ii) In discharges with 1% tritium beam injection, neutron emissivity ratios showed that approximately the same deposition profiles resulted from tritium as from deuterium beams. A thermalized-tritium diffusion experiment was performed in which the tritium-deuterium density ratio was found to be spatially constant across the plasma; in conjunction with similar particle source profiles, this indicates that deuterium and tritium have similar particle transport properties. (iii) In two high performance discharges for which two of the sixteen neutral beam sources operated with 100% tritium, the production rate of 14MeV neutrons reached $6 \cdot 10^{17} n \cdot s^{-1}$. The α-particle 2-D birth profile was directly inferred from the measured 14MeV neutron emissivity profile. Both the axial 14MeV neutron emissivity and the axial ion temperature saturated before the maximum global emission was reached. (iv) During the tritium cleanup phase, residual tritium entering the plasma produced a spatially constant ratio of tritium to deuterium, confirming the similarity of their particle transport properties.

1. INTRODUCTION

During a series of tritium experiments in the Joint European Torus (JET) [1], a comprehensive range of neutron diagnostics [2] was operated to study the neutron emission resulting from d-d and d-t reactions. This paper consists of an analysis of neutron emission profile measurements of JET plasmas that explores the behaviour of tritium ions with energies spanning the energy range from 1keV to 1MeV. The types of discharge discussed in this paper are the same as those described in [1].

In JET deuterium plasmas, the tritium enters the plasma through four different processes: (i) d-d fusion reactions which generate 1MeV tritons, exploited

through burnup studies; (ii) neutral beam injection (NBI) by means of one or two 70-85keV positive ion neutral beam injector sources with a 1% tritium, 99% deuterium mixture, for measurements of deposition profiles of tritium beams and the subsequent diffusion of thermalized tritium; (iii) injection from 2 beam sources with 100% tritium to generate substantial fusion power; (iv) tritium recycling from the walls, during cleanup operations. During this series of experiments, the production rate of 14MeV neutrons varied by several orders of magnitude.

In these experiments [1], the separatrix-bounded plasmas in H-mode predominantly contained deuterium with small, by varying, amounts of tritium together with carbon and beryllium impurities, and exhausted their power mainly into carbon tiles. The plasma parameters were typically current I_p = 3.1 MA, toroidal field B_T = 2.8 T, major radius R_o = 3.15 m, midplane minor radius a_o = 1.0 m, and surface elongation k = 1.7, with q_{cyl} = 2.8.

The JET neutron emission profile monitor provides simultaneous measurements of the line-integrated 2.5MeV and 14MeV neutron emissivities, with both temporal and spatial resolution [3, 4]. Previous 2.5MeV and 14MeV neutron measurements on JET have been summarized by Jarvis [5]. The emissivities from the neutron emission profile monitor were normalized to the instantaneous global neutron emission as measured with fission chambers (2.5 and 14MeV neutrons) and silicon diodes (14MeV neutrons); these, in turn, were normalized to measurements of total neutron yields performed using neutron activation techniques [6]. The key aspects of the neutron emission profile monitor and interpretation of its data are discussed in Sections 2, 3 and 4.

In Section 2, the capabilities of the profile monitor for 2.5 and 14MeV neutron measurements are outlined. For data normalization and interpretation, the tomography computer code NEUTOMO [7, 8] was used to determine the 2-D neutron emissivity profile from the line-integral measurements. In Section 3, the tomographic method is discussed. In the Appendix (the results summarized in Table II of Section 4), it is shown that ratios involving neutron emissivities and fusion reactivities can be used to infer the concentration of thermalized tritium in the plasma, the tritium beam deposition profiles and the deuterium density during triton burnup. This is the first time that the neutron diagnostics and experimental programme have combined to allow the use of these ratios.

The measured profiles of 14MeV neutron emission from 1MeV tritons produced by d-d fusion while slowing down in the deuterium plasma are described in Section 5. These reactions provide an irreducible background of 14 MeV neutron production. Such investigations are relevant to alpha (α) particle physics, since 1MeV tritons have comparable orbits and birth profiles to the α–particles from d-t fusion. These tritons can be detected in the plasma during their slowing-down through fusion reactions which produce neutrons. Triton burnup studies [9-12] have been reported previously.

The behaviour of injected and thermalized tritium in the plasma is examined in Sections 6, 7, and 8 to investigate diffusion of thermalized tritium, fusion power production, and tritium profiles in the plasma resulting from cleanup experiments. In Section 6, tritium beam deposition and thermalized tritium diffusion are examined. A neutral beam with a 1% tritium mixture is injected to provide a central source of tritium ions, which produces a source of 14MeV neutrons strong enough to dominate the triton burnup source. The time evolution of the thermalized tritium density profile is observed after abruptly turning off the 1% tritium neutral beam. The two high fusion power discharges heated and fuelled by 100% tritium from two neutral beam sources and 100% deuterium from fourteen neutral beam sources are discussed in Section 7, showing how the 14MeV neutron emissivity profile evolves. In subsequent cleanup experiments, profile measurements of residual tritium in the plasmas were obtained, as discussed in Section 8. Section 9 contains a summary, and Section 10 specifically discussed the particle diffusion results.

2. THE JET NEUTRON EMISSION PROFILE MONITOR

A schematic drawing of the JET neutron emission profile monitor [3, 4] is shown in Fig. 1. The profile monitor comprises two fan-shaped multi-collimator cameras, with ten channels in the horizontal camera and nine channels in the vertical camera. The neutron detectors were NE213 scintillators and their associated photomultipliers, which sent output pulses to pairs of pulse shape discriminator (PSD) units, one tuned for d-d neutrons and the other for d-t neutrons, to distinguish neutron from γ-ray induced pulses. PSDs have upper and lower energy detection biases set to preferentially detect unscattered neutrons and to reject scattered neutrons. The "d-d" PSDs had an energy window for proton recoil events that spanned 1.9-3.5MeV, and the "d-t" PSDs covered from 7 MeV to about 17MeV.

The intrinsic detection efficiencies of one of the NE213 scintillators for 2.5MeV and 14MeV neutrons were determined empirically using a laboratory accelerator source, and the efficiencies were also calculated. The efficiencies depend on the scintillator geometry and the energy bias setting of the PSD. The setting is monitored by recording the count-rates from a ^{22}Na γ-ray source which is mounted with the scintillator. All detectors have similar efficiencies, with $\approx$3% relative error [2]. These efficiencies (designated laboratory and calculation) are shown later in Table I.

Excluding discharges No. 26147 and 26148, the effect of the 14MeV neutrons on the 2.5MeV neutron measurements was less than 10%, due to the relatively low detection efficiency (0.6%) of the "d-d" PSD channels to 14MeV neutrons. For discharges No. 26147 and 26148 (with 2 neutral beam sources injecting 100% tritium), the global rates of 14MeV neutron production reached $6 \cdot 10^{17} n \cdot s^{-1}$. Immediately prior to No. 26147, the collimation apertures were reduced in size to lower the count-rate due to 14MeV neutrons (these small inserts were left in place for the subsequent tritium cleanup discharges); this did not reduce the signals due to background γ-rays and some breakthrough occurred (γ-rays being erroneously recorded as neutrons) for the edge channels where the γ-ray count-rates exceeded the neutron count-rates. Fortunately, where measurements could be made, the γ-ray signals depended only on total neutron yield. By using the measured total γ + n count-rates, the neutron data could be corrected for breakthrough. For all other discharges, the γ-ray breakthrough was not significant except for the case of channel 11, which had the lease effective shielding.

To obtain the line-integral of the neutron emission along a chord through the plasma, the neutron data appropriate to each detector had first to be corrected for back-scattering from that part of the vacuum vessel wall lying in the line-of-sight, and for detector dead-time, attenuation by port material, collimator scattering and solid angles. The 14MeV neutron back-scattering contribution is negligible.

The effective solid angles and scattering corrections were determined by detailed neutron transport calculations. The statistical accuracy and overall reliability of the calculations degrade as the size of the aperture through the collimators is reduced and as the energy of the source neutron increases. Fortunately, there is a strong degree of commonality between the channels of the separate cameras, so that any discrepancy between calculations and measurements manifests itself as a difference in overall efficiencies between the two cameras (which are of

significantly different design). In practice, as described below, it was found that the calculated camera efficiencies were in agreement with experiment for all but the 14MeV neutron measurements while using small aperture inserts during the high performance discharges and subsequent cleanup discharges. For these discharges, the relative efficiency of the vertical camera had to be reduced by 18% in order to obtain the same volume integral neutron emission as from the horizontal camera.

The viewing extent in the poloidal plane of the plasma is 0.1 m for the central channels and 0.2 m for the edge channels at the region of maximum emissivity along each chord. The projected channel separation in the central region of the plasma is 0.2 m. A time-integrated rate of global neutron emission of 10^{14} n is required to achieve a statistical error of less than 10% of the counts in channels receiving a significant neutron flux, thereby defining the time resolution.

Using the above-mentioned corrections and efficiencies, the line-integrals were inverted to find the local neutron emissivity of the plasma, which was then volume-integrated to obtain the global emissions (the total d-d and/or d-t total yields), which were normalized to fission chamber and Si diode measurements. Both the 2-D NEUTOMO computer code [7, 8] (described in the next section) and the 1-D ORION computer code [9] were used to obtain neutron emissivity profiles. ORION uses flux surfaces from calculated MHD equilibria and assumes them to be surfaces of constant neutron emission. A best-fitting 2-D emissivity profile is generated from a 1-D analytical function of flux for the neutron source with two or three free parameters. An adjustment factor for the efficiencies was obtained by varying them *in common* so as to equalize the global emissions from either code to the fission chamber or Si diode global emissions, which, in turn, had been normalized using the neutron activation system. The neutron emission from these plasmas was fully within the profile monitor's field of view, allowing an accurate normalization to the global emission. The inversion of the data yielded fully self-consistent 2-D neutron emissivity profiles, provided the 18% adjustment mentioned above was introduced for 14MeV, small aperture, measurements. The adjusted efficiencies from both NEUTOMO and ORION are shown in Table I, and are independent of aperture size.

TABLE I

Detection Efficiencies for the Neutron Emission Profile Monitor

NORMALIZATION TYPE AND NEUTRON ENERGY		d-d 1.9-3.5MeV	d-t 7-17MeV
Laboratory	- 2.5MeV	(2.4 ± 0.1)%	(0.0)%
Calculation	- 2.5MeV	(2.5 ± 0.3)%	_____
ORION	- 2.5MeV	(2.2 ± 0.2)%	_____
NEUTOMO	- 2.5MeV	(2.3 ± 0.2)%	_____
Laboratory	- 14.MeV	_____	(1.3 ± 0.2)%
Calculation	- 14.MeV	(0.6 ± 0.5)%	(1.5 ± 0.3)%
ORION	- 14.MeV	_____	(1.8 ± 0.2)%
NEUTOMO	- 14.MeV	_____	(1.8 ± 0.2)%

3. TOMOGRAPHIC ANALYSIS

The tomographic method used in NEUTOMO employs a hybrid pixel/analytic algorithm [8], which involves a poloidal Fourier analysis and a radial Abel inversion, starting from outside and working inwards. NEUTOMO is able to reconstruct accurately a series of test profiles, using the following approach. A standard geometry is chosen for the inversions which consisted of nested elliptical surfaces with a fixed ellipticity of 1.3, centred on a characteristic position near the magnetic axis of major radius R = 3.1 m and height Z = 0.0 m, with a maximum horizontal minor radius of 1.2 m. The X-point plasmas in JET examined here have ellipticities varying from 1.3 on axis to 1.6 - 1.7 at the surface. The emissivity profiles on the near-elliptic contours are described by a 4-term Fourier poloidal expansion and a radial Abel inversion. The analysis code initially smoothes the measured nine or ten channel lines-of-sight, assumed to be of zero width, into synthesized 100-channel signals for each camera before the inversions are performed. (ORION allows for finite viewing width, and Fig. 4.6 of ref. [9] shows the zero width assumption to be adequate for most profiles). Using the emissivity profile deduced from tomography, line-integrals are calculated along the experimental sight-lines for comparison with measured data. The amount of smoothing is chosen to constrain calculated line-integrals to be within ±10% of the experimental data, and to suppress spatial oscillations smaller than the camera resolution. The shape, position and amplitude of the derived

emissivity profiles were found to be relatively independent of the choice of solution geometry, so long as the resultant agreement of actual and calculated line-integrals was within ±10%. The neutron emissivity varies over a fixed ellipticity surface of the solution geometry, owing to the poloidal Fourier representation, to generate 2-D profiles.

Owing to the intrinsic limitations on spatial resolution, the amount of fine structure detail obtainable is limited. Tests using model profiles, including 10% random errors, show that peaked, flat, hollow, outwardly shifted, and hollow with central peak profiles, when reconstructed by 2-D tomography, reproduce the model profiles to an accuracy of ±10%. An advantage of 2-D tomography is that emissivity profile shapes do not require an initial profile specification as in ORION, and do not have to be constant along a flux surface. Thus, hollow profiles and departures from constant emission on a flux surface have been observed with NEUTOMO [7].

As an example of inverting data to obtain the emissivity profile and then reconstructing the line-integrals, the tomographic method of NEUTOMO was applied to the corrected 14MeV neutron profile monitor data for the time interval 13.23 to 13.27 s from the high power discharge No. 26148 [1]. In Fig. 2, a comparison is made between measured line-integrals and those calculated by integrating the neutron emissivity profile which was reconstructed using tomography. The reconstruction is similar to the data from both cameras, showing that a smooth emissivity profile can be obtained. As shown in Table I, an efficiency of 1.8% was obtained by normalizing the measurements so that the integral of the emissivity profile equals the fission chamber rate of $6 \cdot 10^{17} n \cdot s^{-1}$. The scale in Fig. 2 give the corrected absolute neutron flux at the detector, with a maximum of $3.0 \cdot 10^{16} n \cdot m^{-2} s^{-1}$ for the vertical channel number 16.

The TRANSP code [13] has been used at JET to check the internal consistency of all the measured diagnostic data; in addition, it provides an estimate of the fraction of neutrons which was produced for each type of fusion neutron source mechanism on the basis of measured plasma profiles. Neutron measurements are not input to the code, but rather are used as a consistency check. The experimental 14MeV neutron fluxed shown in Fig. 2 are compared in Fig. 3(a) with line-integral emissions calculated for each neutron camera channel from a TRANSP simulation [14] that uses a radially dependent Z_{eff} profile and equal deuterium and tritium particle diffusion coefficients. The TRANSP-calculated

line-integrals plotted in Fig. 3(a) have been normalized (downwards by 9%) to the fission chamber measurements to give a direct comparison of shapes at equal global fusion rates. In Fig. 3(b), the same comparison is made for the 2.5MeV neutrons from discharge No. 26087, and the TRANSP calculation was used directly, without normalization. The agreement is excellent for the 2.5MeV neutron data from discharge No. 26087, except for a relative shift in the horizontal camera data, due to the TRANSP use of a midplane centred equilibrium, whereas the actual plasma position is below the midplane, as shown by the experimental camera data. The agreement between measured 14MeV neutron data and TRANSP simulations in Fig. 3(a) is equally good for the horizontal camera but the experimental data from the vertical camera look a little ragged, presumably a result of the large γ-ray corrections that had to be made.

In what follows, we study tritium behaviour using measured neutron data; some comparisons are made with TRANSP predictions [14] and, where appropriate, some TRANSP-calculated quantities are used, such as the deuterium beam ion contribution to the total deuterium density in the plasma. All discharges here were analysed using NEUTOMO.

4. RATIO METHOD

By using the local 2.5MeV and 14MeV neutron emissivities (R_*) derived from experimental measurements, the ratio of thermal tritium density (n_t) to thermal deuterium density (n_d) can be obtained versus spatial position and time in terms of the fusion reactivities ($< \sigma v >_*$, where * = $_{dd}$ or $_{dt}$), depending on the dominant fusion neutron source mechanism. These ratios are derived in the Appendix and summarized in Table II as eqs. (A.1) and (A.2).

TABLE II
Ratio Methods with 2.5MeV and 14MeV Neutrons

RATIO FORMULA	SOURCE R_{dd}	SOURCE R_{dt}	EQ
$n_t / n_d = (R_{dt} / R_{dd}) / (2 < \sigma v >_{dt,th} / < \sigma v >_{dd,th})$	d-plasma + d-plasma	d-plasma + t-plasma	(A.1)
$n_t / n_d = (R_{dt} / R_{dd}) / (< \sigma v >_{dt,bp} / < \sigma v >_{dd,bp})$	d-beam + d-plasma	d-beam + t-plasma	(A.2)
$D_t / D_d = (R_{dt} / R_{dd}) / 30$	d-beam + d-plasma	t-beam + d-plasma	(A.7)
$n_d / n_e = (R_{dt}(t_o) / R_{dd}(t_o - \Delta)) / (X \cdot H(t_o))$	all d+d reactions	1MeV t + d-plasma	(A.8)

Symbols: density (n); beam deposition rate (D); species: deuterium ($_d$), tritium ($_t$), electrons ($_e$); 2.5MeV neutron emissivity (R_{dd}); 14MeV neutron emissivity (R_{dt}); fusion reactivity ($< \sigma v >_*$); in (A.8), emissivities at times t_o or t_o-Δ; ratio of reactivity branches ($X \approx 0.9$); normalized fractional burnup ($H \approx 0.044$).

The fusion reactivity ratios in equations (A.1) and (A.2) are plotted versus in ion temperature T_i in Fig. 4. Even though the thermal plasma - thermal plasma $< \sigma v >_{*,th}$ variations are strong functions of temperature, their average ratio is 157 with only ±18% variation for $4<T_i<25$keV, so only an approximate ion temperature profile measurement is required. The ratios of $< \sigma v >_{*, bp}$ values are shown for deuterium beam energies of 140keV and 85keV, energies typical of the JET neutral beam sources used in these experiments. The reactivity ratios are only weakly dependent on T_i over the range $8<T_i<25$keV appropriate to beam heating.

In what follows, it is assumed that 2.5MeV and 14MeV neutrons are each produced by one dominant source mechanism, as summarized in Table II. It is possible to improve the approximations embodied in equations (A.1) and (A.2) and (A.2) with (A.3) and (A.4a,b).

Based on equations (A.5) and (A.6), the relative beam deposition rates for tritium and deuterium, D_t and D_d, during neutral beam injection are derived in equation (A.7). The approximations for using equation (A.8) to obtain the ratio of deuterium density to electron density (n_d/n_e) during fusion product triton burnup are described in the Appendix. Equations (A.7) and (A.8) are also summarized in Table II.

The formulae quoted in Table II form the basis of analysis in this paper, and the results are compared with estimates from simulation codes using the full range of plasma measurements.

5. 14MeV NEUTRON BACKGROUND IN d-d PLASMAS

During deuterium discharges, there is a background of 14MeV neutrons from the burnup of slowing-down 1MeV tritons from d-d fusion. This background provided the possibility of testing the neutron diagnostics during experiments producing a high intensity of 2.5MeV neutrons, and of quantifying the level of the associated 14MeV neutron background. A previous study [10] of the spatial width of 14MeV neutron emissivity from triton burnup measurements concluded that it was slightly broader than that of the 2.5MeV neutrons. The 2.5 MeV profiles were measured during the entire high power heating period.

Discharge No. 26087 [1] gave the highest production rate of 2.5MeV neutrons out of several high performance discharges with pure deuterium neutral beam injection into a deuterium plasma. Consequently, the discharge generated the highest production rate of 1MeV tritons. The maximum values of the 2.5 and 14MeV neutron emissivity profiles are presented in Fig. 5. 15MW of high power neutral beam heating was applied from 12 s after discharge initiation, and lasted until 14 s, when the beam power fell to 4MW. The 2.5MeV global neutron emission increased up to $4.3 \cdot 10^{16} n \cdot s^{-1}$ at 13.4 s, then declined rapidly whilst the effective charge Z_{eff} rose steeply. A sawtooth crash at 13.47 s contributed to the fall in global emission. As is shown in Fig. 5, the 14MeV neutron emission persisted for 500 ms before falling.

The 14MeV neutron data were summed over 100 ms intervals to obtain ±10% statistics for tomographic analysis, whereas the 2.5MeV data were summed over 60 ms. In Fig. 5, the maximum neutron emissivity along the major radius chord and the half-width of a gaussian fitted to the data are plotted for both 2.5 and

14MeV neutrons. The profiles are plotted as 1-D midplane cuts through the 2-D profiles versus time in Fig. 6.

Features are apparent from these graphs which confirm conclusions reached previously [9-12]. The observed time delay between the 2.5MeV and 14MeV neutron maximum local emissivity is similar to the calculated classical axial slowing-down time of 1MeV tritons to within measurement and calculation errors. Based on plasma profiles shown in Fig. 5 and Fig. 6, the width of the 14MeV neutron emissivity profile was found to be greater than that of the 2.5MeV neutron emissivity profile during the entire heating period. Similar observations were made previously for the period after the high power heating had terminated.

To find the axial deuterium density, equation (A.8) was applied. An approximate value of the ratio of d-d reactivity for producing (n + ^{3}He) to that for (p + t) is X = 0.90 and the calculated value of the normalized fractional burnup is H = 0.044. The majority of orbits of 1MeV tritons born on the plasma axis are bounded within the inner quarter of the plasma radius. The electron temperature was nearly constant and the 14MeV neutron emissivity profile was relatively flat over this region. The sawtooth crash only reduced the axial emissivity of the 14MeV neutrons to about 80% of the pre-crash value. The axial electron density dropped by about 10%, implying that the fast triton density remained at about (90 ± 10)% of its pre-crash value. The 10% uncertainty propagates into the error in the resulting estimate of the deuterium density. Using the time-delayed ratio of neutron emissivities $R_{dt}(t_o) / R_{dd}(t_o - \Delta)$ for the peak values in time, the density ratio on axis $n_d(t_o) / n_e(t_o)$ equals 0.4 ± 0.1. At time t_o = 13.9 s, radially varying profiles of Z_{eff} measured by CXRS gave an inferred value of $n_d / n_e = 0.57 \pm 0.10$ on axis. TRANSP calculations indicate that about 1/10 of this deuteron density was due to beam ions, but this does not effect the comparison since the triton reactivity is similar for thermal and beam deuterium ions.

The inferences from deduced 14MeV neutron emissivity profiles concerning the diffusion properties of fusion product tritons and their redistribution during sawtooth crashes will form the subject of separate studies.

The effect of the different d-d fusion sources of 2.5MeV neutrons on the amplitude of a sawtooth crash of the neutron emissivity is investigated next. The sawtooth crash at 13.47s has the characteristics of a high-β sawtooth crash [15, 16].

At 13.42s, just before the sawtooth crash, the thermal deuteron density and temperature on axis were $3.8 \cdot 10^{19} m^{-3}$ and 17 keV respectively, having fallen from 19keV slightly earlier. The d-d thermal fusion emissivity on axis was calculated from n_i and T_i to be half of the total axial 2.5MeV neutron emissivity of $2.7 \cdot 10^{15} n \cdot m^{-3} s^{-1}$ deduced from tomography. Just after the sawtooth crash, the axial ion temperature dropped to 11keV at 13.52s, leading to a 50% fall (i.e. $\approx 0.7 \cdot 10^{15} n \cdot m^{-3} s^{-1}$) in thermal fusion emissivity. The total axial 2.5MeV neutron emissivity fell to $1.3 \cdot 10^{15} n \cdot m^{-3} s^{-1}$, implying that half of the decrease was in the beam-plasma and beam-beam contributions due to a redistribution of beam ions.

Before the sawtooth crash, TRANSP calculations gave a total axial 2.5MeV neutron emissivity value of $2.3 \cdot 10^{15} n \cdot m^{-3} s^{-1}$, within 15% of the experimentally deduced value, and the deduced line-integrals from TRANSP of the neutron emission are the same as experimentally measured values to within 10%. The beam-beam contribution was calculated to represent less than 10% of the total axial emissivity, with beam-plasma and thermal fusion contributing approximately equally to the total. Since the total fell by half due to the crash, and since the thermal contribution was calculated to have fallen by half, therefore the beam-plasma contribution also fell by half.

6. BEAM DEPOSITION WITH 1% TRITIUM NEUTRAL INJECTION AND DIFFUSION OF THERMALIZED TRITIUM

A series of discharges were run in which one or two of the 80keV beam sources had a mixture of 1% tritium and 99% deuterium, to study tritium beam deposition and the subsequent diffusion of thermalized tritium. During these discharges, the rate of production of 14MeV neutrons was less than half the rate of the 2.5MeV neutrons, so that it was possible to obtain simultaneous 2.5 and 14MeV neutron emissivity profiles without significant interference of the 14MeV neutrons in the "d-d" PSDs.

For discharge No. 26097 [1], the relative beam deposition profiles of deuterium and tritium were determined using equation (A.7) and the neutron emissivity profiles obtained simultaneously at the turn-on time of the 1% tritium mixture beams, before the build-up of thermal tritium occurred. The profiles of the 2.5 and the 14MeV neutron emissivities were similar in shape, but not in magnitude, hence their ratio was approximately constant across the profile, and

the ratios of overall and local emissivities were the same. The deuterium and tritium beams therefore had similar deposition profiles. Taking into account the various beam energies and known deuterium beam power, the tritium injection power was deduced from the profiles to be 13-15kW per beam source, in agreement with the 1% tritium fraction in the source gas.

A tritium particle diffusion experiment was performed as follows. At 12s into discharge No. 26114, the deuterium beam power was increased to 8MW, and at 12.5s, an additional 1MW, 80keV beam with 1% tritium was switched on, giving an injected tritium power of approximately 13kW, compared to a total injected power of 9MW. The 1% tritium beam was turned off at 13.5s, and replaced with a 1MW beam of pure deuterium. The diffusion of tritium was examined by following the evolution of the neutron emissivity profiles produced by a deuterium beam into a deuterium and tritium plasma after the 1s injection pulse of tritium. In Fig. 7(a) and Fig. 7(b), the neutron emissivity profiles along a radial chord at the tokamak midplane are plotted versus major radius and time for 2.5MeV neutrons and 14MeV neutrons. The shapes of the 2.5MeV and 14MeV neutron emissivity profiles were similar, but the time evolutions were different. After the tritium beam was turned off at 13.5s, the 2.5MeV profile stayed relatively constant for the next second, while the 14MeV profile decayed slowly, but generally maintained the same shape. After a sawtooth crash at 14.085s, there was a temporary flattening of both profiles.

The ratio of n_t/n_d was obtained from equation (A.2) as a function of space and time using a neutron emissivity and beam-plasma reactivity ratios based on a weighted average of the beam energies. The neutron emissivities were sufficiently intense to obtain the density ratio over the inner ±50% of the plasma radius. The first time-interval analyzed is 13.6-13.7s, thereby excluding the beam-plasma contribution from the tritium beam, since the tritium injection ended at 13.5 s. The neutral beam power was composed of 1/4 extracted at 80keV and 3/4 at 140 keV. Axial parameters after 13.6 s were: T_e = 6.2 keV, T_i = 7 keV, Z_{eff} = 2.2, n_e = $4.4 \cdot 10^{19} m^{-3}$ and $n_d = 3 \cdot 10^{19} m^{-3}$ (of which about 10% were fast ions). In Fig. 8(a), the ratio n_t/n_d and its radially-averaged value are plotted versus major radius for two time points during the tritium density decay phase of discharge No. 26114. The data are shown with experimental error bars of ±20%, attributable to error propagation from the line-integral measurements, tomographic inversion and the ratios of the 2.5 and 14MeV neutron emissivities. With experimental errors, the density ratio was constant as a function of major radius

during all time intervals between 13.6 and 14.7s. The electron density profile was relatively flat over the radial region investigated. At 13.7s, the deuterium density profile implied from Charge Exchange Recombination Spectroscopy (CXRS) measurements was also relatively flat, with a value at half the plasma radius equalling 85% of the axial value.

To justify the application of equation (A.2) to the decay phase to find n_t/n_d, it is necessary to show that the neutron emissivity was dominated by beam-plasma reactions. Observations with Si diodes of the global 14MeV emission before 12.5s indicated that the relative contribution from triton burnup after 12.5s should be negligible. The calculated contribution, from n_i and T_i, of thermal d-d fusion to the measured total 2.5MeV neutron emissivity was approximately 1/6. A detailed TRANSP simulation similarly indicated that the axial proportions of the various contributions to the 2.5MeV neutron emissivity were: bp, th, bb = 71%, 18%, 11%; and to the 14MeV emissivity were: bp, th, bb = 79%, 21%, 0%. Beam-beam reactions only affect the results within the level of measurement errors. The effects of these reactions are quantified by using equation (A.4a) for the thermal correction, and the error is only 4%. Using TRANSP calculations for all the contributions to the fusion neutrons, including beam-beam, the corrected values of n_t/n_d deduced from using equation (A.4b) are 1.13 times the values from equation (A.2). The effect of plasma rotation, as discussed in the Appendix, is less than 1%.

The observation that the 2.5 and 14MeV neutron emissivity profile shapes were the same, even after the sawtooth crash, is now easily understood. Since the neutron production was mostly from beam-plasma reactions in a plasma with relatively flat density profiles, each emissivity profile depended mainly on the thermalizing beam-injected deuterium ions, and consequently both emissivity profiles kept similar shapes while the tritium density decayed.

In Fig. 8(b), the radially-averaged density ratio n_t/n_d is plotted as a function of time. The fitted exponential curve has a 1.0 s decay. The initial value of n_t/n_d is $3 \cdot 10^{-4}$, a reasonable value since about 10^{-3} of the injected beam particles were tritium, and additional pure deuterium was added by gas puffing. The trend of the exponential decay was not affected by the sawtooth crash at 14.085s which temporarily flattened the emissivity profiles.

Since n_t/n_d was constant across the profile, it could also be obtained from the ratio of the global 14MeV to 2.5MeV neutron emissions. Because the emissivity ratio is a weak function of ion temperature, the reactivity ratio corresponding to the central ion temperature can be used. The global emission value were obtained from fission chamber and Si diode measurements. The n_t/n_d obtained using these global neutron emission rates differed from the radially-averaged n_t/n_d from local neutron emissivity rates shown in Fig. 8(b) by no more than ±20%.

A cylindrical approximation of the global particle diffusion coefficient for tritium gives $D \equiv a^2 / 5.6\tau_{dec} = 0.2 m^2 / s$ where $\tau_{dec} = 1.0$ s is the observed time decay constant of the thermalized tritium density. Based on the experimental observations that the deuterium and tritium beams had similar spatial deposition profiles, and that the density ratio n_t/n_d was spatially constant, a reasonable hypothesis is that thermalized deuterium and tritium have approximately the same diffusive behaviour. The radial profile of the diffusion coefficient has been calculated [14] using TRANSP to predict the 2.5 and 14MeV neutron emissivity profiles with different particle mixing models. Two diffusive models were able to reproduce the observed neutron emissivity profiles. One was a spatially constant fraction model of tritium to deuterium density, while the other was that tritium and deuterium had the same particle diffusion coefficients. It was possible to reject mixing models in TRANSP in which tritium and deuterium particle diffusion coefficients differed by a factor of 2. Calculations with TRANSP also indicated that the beam deposition profiles for deuterium and tritium should be similar, as found above.

Discharge No. 26095 was part of the series of discharges with 1% tritium injection. At the peak neutron emission at 13.7s, the ratio R_{dt}/R_{dd} of both global and axial neutron emissivities was 0.2. The axial ion parameters [1] correspond to a production rate of 2.5MeV neutrons from thermal fusion of two-thirds of the tomographically deduced total value of $2.8 \cdot 10^{15} n \cdot m^{-3} s^{-1}$. Since in this case thermal fusion was dominant, equation (A.1) gives n_t/n_d = 0.08%. The baseline correction to the 14MeV rate due to tritium beam - deuterium plasma was less than 10%, and was ignored. This n_t/n_d value is the same as that calculated by TRANSP [1].

7. HIGH FUSION POWER EXPERIMENTS

Following the above-mentioned experiments, there were two discharges, No. 26147 and 26148 [1], with two of the sixteen beam sources injecting 100% tritium beams. The resulting 14MeV neutron global rates reached $6 \cdot 10^{17} n \cdot s^{-1}$. Tomographic inversion of the neutron data was performed to obtain the 2-D emissivity profiles at twelve regular intervals, presented in Fig. 9 as colour contour plots. The 14MeV neutron emissivity is plotted versus major radius and height, with 10 ms time bins shown at 150 ms intervals, covering the high power heating phase from 12.10s to 13.75s.

The neutron emission profile monitor implicity functions as a diagnostic of the α-particle birth profile. Fig. 9 therefore also shows the birth profile in space and time of the α-particle accompanying neutron production from the d-t reaction. The inferred maximum in space and time of the α-particle production power was 14 $kW \cdot m^{-3}$ (70 $kW \cdot m^{-3}$ for α-particles plus neutrons), which was small compared to the neutral beam deposition power.

In Fig. 10, time-dependent plots are shown of (a) the maximum local emissivity and (b) the global 14MeV neutron emission, during the high power heating phase form 12 to 14s. As shown by Fig. 9 and Fig. 10, the neutron emissivity initially increased and then, due to the first sawtooth crash, decreased on axis and flattened. After the crash, the emissivity again increased on axis, rapidly at first, and then saturated, as did the axial ion temperature, when the global emission reached 2/3 of its maximum value. The neutron emissivity profile continued to broaden and the global neutron emission continued increasing up to a maximum value of $6 \cdot 10^{17} n \cdot s^{-1}$ (as determined from fission chamber measurements). This phase was terminated by another crash, after which the axial ion temperature decreased and a strong impurity influx occurred. The neutron emissivity peaked spatially again, but at a lower level which continued to fall along with the central ion temperature.

Interpreting the behaviour of the neutron emissivity requires a knowledge of the d-t fusion neutron source mechanisms. however, since 2.5MeV neutron emissivity profile measurements could not be extracted because of the dominant 14MeV neutron flux (see Table I), the ratio methods discussed previously could not be used. For this reason, the discussion in this paper is confined to the sawtooth crash at the maximum neutron emissivity, making use of TRANSP

simulations for fusion neutron source contributions before the crash. Furthermore, detailed TRANSP simulations indicate that the fraction of axial deuterium density due to fast ions is greater than 10%, and the sum of beam-plasma contributions from both deuterium and tritium beams exceeded the thermal contribution on axis.

The sawtooth crash at the maximum emissivity at 13.285 s, is now examined. In Fig. 11, 2-D emissivity profiles of the 14MeV neutrons are displayed versus major radius R and height z for 2.5ms time bins, (a) at 13.28s, just before the sawtooth crash, and (b) at 13.29s, just after the crash, for discharge No. 26148. The peak emissivity at a major radius of 3.2m attained a value of $2.5 \cdot 10^{16} n \cdot m^{-3} s^{-1}$, just before the crash. Just after the crash, the emissivity profile became hollow, with hollow and crest emissivities of 1/3 and 2/3 of the pre-crash maximum, respectively. The electron and ion density and ion temperature profiles were changed from slightly peaked to slightly hollow by the sawtooth crash. The axial T_i dropped from 19 to 13keV, corresponding to a fall in the d-t thermal fusion reactivity by 1/2, contributing to less than half of the change in the observed axial neutron emissivity, but comparable to the fall in the global neutron emission. TRANSP calculations indicate that before the sawtooth crash, the thermal and beam-plasma contributions were comparable near the axis, and that beam-beam fusion contributed about half as much as either of the other sources. The remainder of the axial emissivity crash must therefore have been due to a redistribution of the fast beam ions from the axis to an intermediate plasma radius, thereby leading to the observed hollow neutron emissivity profile, but not contributing to a fall in the global neutron emission. The beam-beam contribution is also known [7] to drop strongly during a crash. The behaviour of this sawtooth crash is similar to crashes in discharges without tritium which have similar contributions from thermal beam-plasma and beam-beam reactions.

8. PROFILE MEASUREMENTS DURING TRITIUM CLEAN-UP

The tritium density profiles were monitored during the initial tritium cleanup discharges in order to verify the use of global 14MeV neutron emission for tritium concentration measurements, to quantify the effects of contributions from residual tritium and triton burnup and to obtain information on tritium diffusion properties in the plasma. The first fourteen similar discharges from No. 26150 to No. 26165 were analyzed (Nos. 26149, 26158 and 26161 did not occur). Two or three half-second bursts of 2 MW of deuterium neutral beams at 140keV

were added to probe the tritium density in the plasma by giving an enhanced, beam-plasma dominated neutron yield for obtaining n_t/n_d from equation (A.2).

Small collimators had been inserted in the neutron emission profile monitor for the two high power discharges, and these remained during the cleanup experiments. It was therefore necessary to integrate from 8 to 18 s, over the beam pulses and over the intervening ohmic phases of each discharge, to obtain ±10% statistics for the 14MeV neutron emissivity. The 2.5 and 14MeV neutron emissivity profiles were found by tomographic inversion to have the same shape. Examples are shown in Fig. 12 for the first and last discharges in the series studied, Nos. 26150 and 26165, where the local 2.5MeV and 14MeV neutron integrated yields per unit volume derived from tomography are plotted. The 2.5 and 14MeV profiles maintained similar shapes, although different for the two discharges, as the quantity of tritium released from the walls diminished. The ratio of emissivities is constant across the profile, and therefore the ratio n_t/n_d is constant throughout the plasma. Equation (A.2) is therefore applicable to either the local emissivities or to the ratio of global fusion yields from the Si diodes and the fission chambers, so long as beam-plasma fusion from the deuterium beam on the d and t plasma components is the dominant process.

Since almost all the deuterium and tritium enter the plasma at its boundary (either from gas puffing or wall release) with only a very low level density increase (≈5%) from neutral beam injection, the spatially constant density ratio n_t/n_d provides further evidence that deuterium and tritium have similar particle diffusion properties, as follows. It has been observed [17, 18] that the particle flux Γ for electrons and impurities can be described by the equation

$$\Gamma_x = -\delta_x \nabla n_x + n_x \upsilon_x$$

with diffusion coefficients δ_x and pinch velocity υ_x, and that the ratio δ_x/υ_x is the same for all species $_x$. In the relatively stationary condition of these cleanup discharges with surface fuelling, Γ_x becomes small and δ_x/υ_x approximately equals $\nabla n_x / n_x$ for each species. The electron density profile is more rounded in these cleanup discharges than the relatively flatter profiles observed in discharges No. 26114 and No. 26148, and ∇n_x is non-zero. Since both density profiles have the same shape and hence the same $\nabla n_x / n_x$ profile, $\delta_t / \upsilon_t = \delta_d / \upsilon_d$ is indeed obtained.

At low levels of residual tritium, burnup of 1MeV tritons from d-d fusion cannot be neglected. The effect on the emissivity ratios can be quantified by examining the global emission data, which had better time resolution in these discharges. The time-dependencies and magnitudes of the global 2.5MeV neutron emission, measured by the fission chambers, were similar for all the discharges. The 14MeV neutron emission rates measured by the Si diodes had the same time dependence as the 2.5MeV neutrons on the first cleanup discharge No. 25150. The 14MeV neutron yield was reduced on each successive discharge, and discharge No. 26165 showed a time delay which could be attributed to burnup, where the emissivity ratios were becoming close to levels characteristic of triton burnup.

The effect of triton burnup is quantified in Table III, where the 14MeV to 2.5 MeV neutron emissivity ratios R_{dt}/R_{dd} are shown for different time intervals and discharges, comparing local and global ratios. In discharges No. 26150 and No. 26165, one of the beam pulses lasts from 8.5 to 9.0 s, when the neutron emissivity is beam-plasma dominated. In No. 26150, the ratio R_{dt}/R_{dd} is the same for all time intervals and for global and local emissivities. However, in No. 26165, the ratios from integration periods 8.5-9.5 or 8-18s, which include burnup contributions, are about 20%-40% larger than the ratio obtained during 8.5-9.0s, coinciding with the beam pulse, when deuterium beam-tritium plasma reactions are dominant, and fusion reactions from tritons slowing down from 1MeV are delayed until the next 0.5s time slot. For comparison, the ratio from the high performance, deuterium only discharge No. 26087 is given to illustrate the approximate level characteristic of the triton burnup contribution.

TABLE III

14MeV to 2.5MeV Neutron Emissivity and Global Emission Ratios

DISCHARGE	GLOBAL 8-18 s	GLOBAL 8.5-9.0 s	GLOBAL 8.5-9.5 s	LOCAL 8-18 s
26087	0.018	----	----	----
26150	0.22	0.22	0.23	0.20
26165	0.032	0.023	0.028	0.035

Emissivity profile analysis showed the tritium to deuterium ratio to be constant across the plasma in these discharges, so global emission ratios could be used to determine n_t/n_d. The ion temperature was taken to be the central ion

temperature, so $n_t/n_d = (R_{dt}/R_{dd})/220$ based on equation (A.2). The values of R_{dt}/R_{dd} for the time-integrals of the global neutron emission from Si diodes and fission chambers for 8.5-9.0s gave n_t/n_d values which are plotted on a semi-log scale in Fig. 13, where the error bars are approximately ±20%. n_t/n_d decreases approximately exponentially by an order of magnitude during the first fourteen cleanup discharges. Also shown in Fig. 13 as diamonds are the density ratios from the local emissivity ratios from 8-18s in No. 26150 and No. 26165, with the long integration times required for statistical accuracy, illustrating (for No. 26165) the error introduced by triton burnup contributions. A more complete analysis of tritium cleanup experiments including the type of data shown in Fig. 13, but for longer integration times, has been reported separately [19].

9. SUMMARY

Using neutron emission profile measurements, analysis methods based on reactivity ratios were applied to a series of similar discharges with high d-d and varying d-t neutron production rates. The 2-D neutron emissivity profiles were obtained from tomography , and the response of these profiles to heating, diffusion, sawtooth crashes, and impurities was observed. The ratios of 2.5 and 14MeV neutron emissivities and the fusion reactivities were used to deduce the relative tritium to deuterium beam deposition rates and the ratio of thermalized tritium to deuterium density, independently of other plasma measurements. In all experiments except for fusion product triton thermalization, the neutron emissivity profiles from 2.5MeV and 14MeV neutrons were observed to have the same shape, although the shapes and magnitudes varied in time. The implications for particle diffusion are discussed in the next section.

Observations of the burnup of 1MeV tritons from d-d fusion show that 14MeV profiles are broader than 2.5MeV profiles during the entire heating period and are only weakly affected by a sawtooth crash. The deuteron density deduced from equation (A.8) is within error bars of CXRS observations. These profile measurements are consistent with previous investigations in showing classical triton thermalization and little radial transport. The fall after the sawtooth crash in the axial 2.5MeV neutron emissivity, resulting from equal falls in the thermal and beam plasma sources, was significantly larger than that of 14MeV neutrons.

A series of discharges was run using one or two of the 80keV positive ion neutral beam sources with a 1% mixture of tritium in a deuterium beam. During

injection, the shapes of the 2.5 and the 14MeV neutron emissivity profiles were similar, hence the ratio of the emissivities was roughly constant across the profile. Using equation (A.7), beam deposition profiles were shown to be similar for deuterium and tritium beams, as in TRANSP calculations.

14MeV neutron rates up to $6 \cdot 10^{17} n \cdot s^{-1}$, corresponding to fusion powers of up to 1.7 MW were produced in two discharges with two injectors using 100% tritium. The profiles of the 14MeV neutron emissivity showed the effects of heating, sawteeth, and impurity influx, and also gave a measurement of the birth profile of α-particles from d-t fusion. High power heating caused an initially peaked 14MeV neutrons emissivity profile, which was flattened by a sawtooth crash. The axial emissivity subsequently increased to its maximum after 0.5s and then saturated (as did the axial ion temperature), while the profile continued to broaden during a further 0.4s, and the global emission continued to increase. A second sawtooth crash again flattened the profile, which subsequently peaked in shape but kept decreasing in amplitude (along with the central ion temperature) due to a strong influx of impurities. The effect of a major MHD event near the maximum global neutron emission was a relative reduction of the thermal contribution near the axis of comparable magnitude to the fall in global emission, and a redistribution of the dominant beam-plasma fusion source from the axis to an intermediate radius. This behaviour is similar to that observed in discharges without tritium which have similar contributions from thermal, beam-plasma, and beam-beam reactions.

During the first fourteen cleanup discharges, the tritium content of the plasma decreased by an order of magnitude. Based on neutron emissivity profile measurements, n_t/n_d was shown to be spatially constant, which justifies the use of the ratio of global neutron emission to obtain the tritium to deuterium density ratio. The potentially confusing effects of triton burnup on these results were calculated.

In summary, a self-consistent description of tritium behaviour in the plasma has been obtained by applying ratio methods and TRANSP analysis to diagnostic measurements. Within experimental errors, deuterium and tritium are found to behave similarly, and the fusion yields are as expected for the measured plasma and beam parameters.

10. DISCUSSION OF PARTICLE DIFFUSION

In a tritium diffusion experiment, the 1% tritium neutral beam was turned off abruptly and the subsequent evolution of the neutron emissivity profiles was observed. The 2.5MeV profile stayed relatively constant, while the 14MeV profile decayed slowly, both profiles keeping the same shape. Using equation (A.2) the density ratio n_t/n_d was found across the plasma and to decrease exponentially with a 1 s time constant after termination of the tritium beam injection. Analysis of the tritium cleanup discharges indicated that the relative particle diffusion properties of deuterium and tritium could be described by $\delta_t / \upsilon_t = \delta_d / \upsilon_d$, since $\nabla n_x / n_x$ was the same for both density profiles. In this section, we will demonstrate that the particle diffusion in the 1% tritium mixture experiment can be similarly described.

The continuity equation for particle diffusion is given as:

$$\frac{\partial n_x}{\partial t} + \nabla \cdot \Gamma_x = S_x, \text{ where } \Gamma_x = \delta_x \nabla n_x + n_x \upsilon_x$$

where S_x is the particle source rate and all quantities are a function of radius and time. By integrating over a volume enclosed by a magnetic flux surface of area A, using the divergence theorem to convert the volume integral of $\nabla \cdot \Gamma_x$ to $\Gamma_x A$, substituting for Γ_x, dividing by n_x and assuming that n_x can be brought inside the integral in the region of interest (due to a relatively flat density gradient), and defining $L_x = n_x / \nabla n_x$, we obtain

$$\upsilon_x - \frac{\delta_x}{L_x} = \frac{1}{A} \iiint_V \left[\frac{S_x}{n_x} - \frac{1}{n_x} \frac{\partial n_x}{\partial t} \right] dV$$

The integral can be evaluated separately for deuterium and tritium during the tritium decay phase of discharge No. 26114. For deuterium, the neutral beam source and gas puffing are used to maintain the density nearly constant, so $\partial n_x / \partial t \approx 0$ Near the plasma axis, the thermal deuterium density is $n_d \approx 3.5 \cdot 10^{19} m^{-3}$, and $S_d \approx 3.5 \cdot 10^{19} m^{-3} s^{-1}$ from beam deposition calculations, so the kernel of the integral equals $1.0 \cdot s^{-1}$.

For tritium, the beam source was stopped, so $S_t \approx 0$ in a small volume near the plasma axis where the recycling source is negligible. While the deuterium density

profile was held nearly constant, the ratio of n_t/n_d was observed from neutron emissivity measurements to remain spatially constant and decay exponentially with a 1.0s time constant. Thus the kernel of the integral of the tritium equation also equals $1.0 \cdot s^{-1}$, and near the axis:

$$\upsilon_d - \frac{\delta_d}{L_d} = \upsilon_t - \frac{\delta_t}{L_t} = \frac{1}{A}\iiint_V \left[\left(1.0 \cdot s^{-1}\right)\right] \, dV$$

Since L_d and L_t have been measured to be equal, and using the result from the cleanup discharges that $\delta_t / \upsilon_t = \delta_d / \upsilon_d$ when the kernel in the integral was zero, the equalities $\upsilon_d = \upsilon_t$ and $\delta_d = \delta_t$ can be derived directly.

In the regions further from the axis, the beam deposition profile is more peaked than the density profile, so the kernel of the integral is not constant, and the integrals for the deuterium and tritium equations begin to diverge. The neutron measurements themselves are only valid for the inner half of the plasma. Therefore, an off-axis analysis is not attempted here.

In conclusion, within the measurement limits and over a limited spatial range near the plasma axis, the results of both the 1% tritium mixture diffusion experiments and the cleanup discharge analysis are consistent with the particle diffusion and velocity terms of deuterium and tritium being equal to each other. Given the level of experimental errors in determining the plasma density profile, ≈20%, the diffusion coefficients could have a weak mass dependence, for example $(m_t/m_d)^{0.5} = 1.22$, which would not be detected. The neutron emission profiles provided the basis for detailed plasma transport analysis [14], in which results agreeing with those derived from equation (A.2) were obtained.

APPENDIX. RATIO METHODS FOR SOURCE RATES AND DENSITIES

The ratio of thermal tritium density (n_t) to thermal deuterium density (n_d) can be obtained as a function of the fusion reactivities ($< \sigma v >_*$, where * = dd or dt), and local neutron emissivities (R_*). These emissivities are inferred from profile monitor measurements by tomographic calculations for 14MeV (R_{dt}) and 2.5MeV (R_{dd}) neutrons. The only other data required to find n_t/n_d are approximate measurements of the ion temperature. The ratio R_{dt}/R_{dd} can also be used to calculate the tritium beam deposition profile during injection or to analyse triton burnup.

Several methods of analysis are possible, each using a different ratio, each with a separate domain of applicability. The particular ratio chosen depends on the dominance of a particular fusion neutron generation mechanism, i.e. thermal, beam-plasma or beam-beam. General conditions for the dominance of one type of fusion neutron source mechanism and examples with TRANSP [13] calculations are discussed [20]. In the discharge intervals considered here, either thermal or beam-plasma reactions can be dominant. When both are important, a combined method can be used. To determine the dominant fusion neutron source mechanism, two approaches are possible:

1) A full transport simulation with TRANSP.

2) Using n_d and T_d measured by Charge Exchange Recombination Spectroscopy (CXRS) or other diagnostics, the local value of the neutron emissivity due to thermal fusion can be directly calculated. Using tomography, the actual neutron emissivity can be derived. Hence, the fraction due to the thermal fusion contribution is found, indicating whether thermal or beam-plasma is dominant.

A complication is that n_d is the sum of both thermal and fast ion contributions. Approach 2) can be refined by a calculation or measurement (see below) of beam deposition and a local calculation of the beam slowing-down time to determine both the fast ion density and the beam-plasma fusion contribution to the local neutron emissivity (also below).

In deuterium plasmas without tritium injection, 1MeV tritons are produced at the same location and at approximately the same rate as 2.5MeV neutrons due to

the d-d reaction having two branches of almost equal probability. These tritons may undergo t-d fusion reactions while slowing down, generating 14MeV neutrons. The reactivity ratio can also be used to determine n_d/n_e in these discharges, where n_e is the electron density. The 14MeV neutron emissivity from triton burnup is negligible compared to other 14MeV fusion neutron source mechanisms during the tritium injection experiments.

In this work, the fusion reactivities are determined as follows. For beam slowing-down on a Maxwellian plasma, the rate of energy loss due to each ion species, hydrogenic or impurity, and electrons is calculated using the G_e, G_i, and $\ln \Lambda$ functions of Spitzer [21]. The fusion reactivity is calculated by integration over the slowed down distribution and the target ion distribution function. Fusion cross-sections are taken from [22]. In the following, only the full energy components of the beams will be considered. It has been verified that the lower energy components have little effect for the plasmas studied here.

AP.1 THERMAL EMISSION

In a plasma with dominant thermal reactivities $<\sigma v>_{dd,th}$ and $<\sigma v>_{dt,th}$ (shown in Fig. 4), the local neutron emissivities are given by $n_d^2 <\sigma v>_{dt,th}/2$ and $n_d n_t <\sigma v>_{dt,th}$. The density ratio of thermal tritium to deuterium is obtained from:

$$\frac{n_t}{n_d} = \left[\frac{R_{dt}}{R_{dd}}\right] \Big/ \left[\frac{2<\sigma v>_{dt,th}}{<\sigma v>_{dd,th}}\right] \qquad (A.1)$$

AP.2 BEAM-PLASMA EMISSION

In a plasma with dominant beam-plasma reactivities $<\sigma v>_{dd,bp}$ and $<\sigma v>_{dt,bp}$ of a deuterium beam onto a mixed deuterium and tritium plasma (shown in Fig. 4), the ratio is:

$$\frac{n_t}{n_d} = \left[\frac{R_{dt}}{R_{dd}}\right] \Big/ \left[\frac{<\sigma v>_{dt,bp}}{<\sigma v>_{dd,bp}}\right] \qquad (A.2)$$

In tokamak plasmas, plasma rotation can have an important effect (up to 20%-40%) on the beam-plasma reactivity and on the global neutron yield, as discussed in [23]. The effect of plasma rotation on the reactivity is to give the beam ions on

passing orbits near the plasma axis a lower energy in the rest frame of the rotating plasma ions, thereby reducing $<\sigma v>_{bp}$. However, equation (A.2) uses the ratio $<\sigma v>_{dt,bp}/<\sigma v>_{dd,bp}$ which remains nearly unchanged, so the effect of rotation on the estimate of n_t/n_d becomes negligible. For beam ions far from the axis on trapped orbits, the rest frame beam energy is alternately increased and decreased, oscillating in the co- and counter-directions. However, the ratio of the $<\sigma v>$'s remains nearly unchanged. In discharge No. 26114, the rotation velocity was $2.8 \cdot 10^6 m \cdot s^{-1}$, about 1/4 of the plasma sound speed. With 80 keV deuterium beam injection, those deuterons going into passing orbits near the plasma axis will have a relative energy of 69 keV in the rotating frame of the plasma ions. The effective beam energy caused drops of 20% in both $<\sigma v>_{dt,bp}$ and $<\sigma v>_{dd,bp}$, but the ratio changed by less than 1%. Similarly, there is little change in the ratio of reactivities for ions falling into trapped orbits. Having shown that the effect of plasma rotation is negligible on the ratios, we henceforth ignore it.

AP.3 COMBINED BEAM-PLASMA AND THERMAL EMISSION

In deuterium beam-heated plasmas, the neutron emissivity is due to a mixure of beam-plasma, thermal and beam-beam reactions. The ratio of the total emissivities is given by:

$$\frac{R_{dd}}{R_{dt}} = \frac{R_{dd,bp} + R_{dd,th} + R_{dd,bb}}{R_{dt,bp} + R_{dt,th} + R_{dt,bb}} \tag{A.3}$$

We consider cases where the beam-beam fractional contribution is either:
a) negligible or
b) small.

a) By factoring out the leading terms on the right-hand side of (A.3) as in equation (A.2) and by rewriting the factored R_{bp} terms as $(R-R_{th})$, equation (A.3) may be rewritten to obtain n_t/n_d by using n_t/n_d from equation (A.2) for beam-plasma dominated emissivities as a first approximation:

$$\frac{n_t}{n_d} \cong \left[\frac{n_t}{n_d}\right]_{eq(A.2)} \cdot \left[\frac{1 + \left[\frac{1}{\frac{R_{dd}}{R_{dd,th}} - 1}\right]}{1 + \left[\frac{1}{\frac{R_{dt}}{R_{dt,th}} - 1}\right]}\right] \tag{A.4a}$$

In equation (A.4a), R_{dd} and R_{dt} are obtained from tomographic inversion of the emissivity profiles, $R_{dd,th}$ from CXRS measurements of n_d and T_i using the thermal reactivity, and $R_{dt,th}$ from the equation (A.2) estimate of n_t. Since n_d is a sum of fast and thermal ion contributions, using the total n_d in equation (A.4a) is a further approximation valid only when n_f/n_d is small, where n_f is the fast deuteron density, consistent with a small beam-beam contribution.

b) If a separate calculation has been made of the beam-beam contribution, for example with TRANSP, then when this contribution is small, equation (A.4a) can be written to include the beam-beam contribution to the 2.5MeV emissivity:

$$\frac{n_t}{n_d} \cong \left[\frac{n_t}{n_d}\right]_{eq(A.2)} \cdot \left[\frac{1+\left[\frac{1}{\frac{R_{dd}-R_{dd,th}-R_{dd,bb}}{R_{dd,th}+R_{dd,bb}}}\right]}{1+\left[\frac{1}{\frac{R_{dt}}{R_{dt,th}}-1}\right]}\right] \qquad \text{(A.4b)}$$

AP.4 BEAM DEPOSITION PROFILES

It is also possible to determine the relative beam deposition profiles of tritium and deuterium beams. When a tritium beam is initially turned on, in the presence of deuterium beams, the 14MeV neutrons predominantly arise from tritium-beam - deuterium-plasma reactions, provided the fast deuteron density is small compared to the density of thermal deuterons, and that other sources of tritium are negligible. It is also necessary for the 2.5MeV neutrons to be primarily due to deuterium-beam - deuterium-plasma reactions, with the ion temperature low enough that the thermal d-d contribution is not significant. Once the fast ion distribution function has reached steady-state (after a slowing-down time for beam ions), the ratio of the 14MeV neutron emissivity to the emissivity from the d-d beam-plasma 2.5MeV neutrons is:

$$\frac{R_{dt}}{R_{dd}} = \left[\frac{D_t}{D_d}\right] \cdot \left[\frac{n_d \tau_t < \sigma v >_{dt,t-beam,bp}}{n_d \tau_d < \sigma v >_{dd,d-beam,bp}}\right] \qquad \text{(A.5)}$$

where D_t and D_d are the local beam deposition rates of the tritium beam and the deuterium beam in particles/m^3s, and τ_d and τ_t are the deuterium and tritium beam slowing-down times.

D_d and D_t can be obtained individually if an adequate measurement is available of n_d in addition to measurements of T_i, R_{dt}, and R_{dd} to calculate $\tau_* < \sigma v >_*$. Subtracting the calculated fast ion densities $D_d\tau_d$ and $D_t\tau_t$ from the total densities gives the thermal ion density. For 80 keV tritium beams and 140 keV deuterium beams on a deuterium plasma, the ratio of the $\tau < \sigma v >$ values in the right-hand side varies weakly for a wide range of plasma temperature as follows:

$$\text{Defining } F \equiv \frac{\tau_t < \sigma v >_{dt,t-beam,bp}}{\tau_d < \sigma v >_{dd,d-beam,bp}}, \text{ we obtain:}$$

$$30 < F < 33, \text{ in the range } 2.5 \text{ keV } < T_e = T_i < 25 \text{ keV} \qquad \text{(A.6)}$$

In the case of very different electron and ion temperatures, for T_e =5 keV and T_i = 25 keV, the ratio F equals 43. When T_e and T_i are nearly equal, a good approximation to equations (A.5) and (A.6) is:

$$\frac{D_t}{D_d} = \left[\frac{R_{dt}}{R_{dd}}\right] / 30. \qquad \text{(A.7)}$$

AP.5 BEAM DEPOSITION CORRECTION

In a discharge with continuous tritium injection, the thermal tritium density can build up to significant levels. Equation (A.2) for determining n_t/n_d may still be applied by subtracting the contribution due to the tritium-beam - deuterium-plasma reactivity, determined as follows:

When tritium injection begins, the 14MeV neutron emissivity due to tritium-beam - deuterium-plasma reactions establishes an initial temporal plateau level after at least one beam slowing-down time, which serves as a baseline. During the heating of the discharge, this baseline value, at constant tritium beam power and constant (n_d/n_e), is relatively independent of variations in electron temperature and density, since the tritium thermalizes primarily on ions. The tritium-beam - deuterium-plasma reactivity is only weakly dependent on ion temperature, so the baseline correction can be scaled with ion temperature while the neutron

emissivity increases. For ion temperatures of 5, 15, and 25 keV, the scaling multipliers are 1.0, 1.6, and 2.2, respectively. The scaled baseline correction can then be subtracted from R_{dt} in either equations (A.1) or (A.2), depending on the dominant fusion neutron source mechanism. Since the initial plateau value is a small fraction of the maximum emissivities, the correction is also small.

AP. 6 EXTRAPOLATION

Based on equations (A.1), (A.2), and (A.4a,b), Q_{dd} from d-d discharges, the ratio of fusion power to heating power [1], can be extrapolated to Q_{dt} for d-t discharges with 140 keV deuterium and 160 keV tritium beams for heating, and with a 50:50 d-t fuelling mixture. Over a wide range of high performance JET discharges, the ratio of the 14MeV neutron rate to the 2.5MeV neutron rate for 50:50 d-t fuelling is 88, and the ratio of Q_{dt} to Q_{dd} is 210, even with variable amounts of thermal or beam-plasma neutron sources. These ratios were confirmed by comparison with TRANSP simulations [1] and provide a rapid means of extrapolating from present to future plasma performance.

AP. 7 DEUTERIUM DENSITY

The emissivity ratio R_{dt}/R_{dd} can also be used to determine the deuterium density by observation of the triton burnup probability, as was done previously with global measurements of triton burnup [24]. In previous studies on JET [9-12], global measurements of 14MeV neutron emissivity, from triton burnup, showed that the 14MeV neutron peaked later than the 2.5MeV neutron emission, since 1MeV tritons from the d-d reaction must slow down before the maximum d-t reactivity is reached at about 0.2MeV. The triton slowing-down time for normal discharges, typically a few hundred ms, was observed to be classical within measurement errors.

The deuterium density during triton burnup may be determined under the following conditions:

(i) the time evolutions of the local 2.5 and 14MeV neutron emissivities have a similar shape, but are displaced in time by Δ;
(ii) the plasma parameters are approximately constant during the interval Δ;
(iii) the fast triton orbits do not migrate from their regions of birth, and plasma parameters do not vary strongly over the orbits.

Condition (i) is most easily satisfied in discharges where the 2.5MeV neutron emission occurs in a brief burst, which gives a peak in the 14MeV neutron emission when the resulting MeV tritons slow down to the peak of the d-t reactivity cross section. This occurs in many hot-ion H-modes.

Condition (iii) is satisfied in the central regions of the plasmas discussed here when the electron temperature profile is relatively flat near the axis, since tritons born on axis have orbits confined near the axis. Under these restrictions, the local values of n_d at time (t_o) is:

$$\frac{n_d(t_o)}{n_e(t_o)} = \left[\frac{R_{dt}(t_o)}{R_{dd}(t_o - \Delta)}\right] / \left[X \cdot H(t_o)\right] \qquad (A.8)$$

with $H(t_o) \equiv n_e \tau_{ts} < \sigma v >_{triton} (t_o)$, where τ_{ts} and $< \sigma v >_{triton} (t_o)$ are the 1MeV triton slowing-down time and time averaged reactivity respectively, and $X \approx 0.9$ is the ratio of 1MeV triton production to 2.5MeV neutron production from d-d fusion. H is insensitive to the effect charge Z_{eff} and T_i and equals 0.043 ± 0.008 in the range 6 keV $<T_e<$10 keV. With a measurement of n_e, the value of n_d can be obtained from equation (A.8).

AP. 8 GLOBAL RATIOS

When the global emissions for 2.5MeV and 14MeV neutrons are measured simultaneously with fission chambers and Si diodes, respectively, the above arguments can be applied to give a global ratio to be used when local emissivities are not available. The global emission is typically dominated by the central region of the plasma, which has the highest ion temperature and fast ion density. n_t/n_d can be determined in this region using the ratio of global emissions in place of local emissivity ratios. The method is least inaccurate when local emissivity radial profiles of 2.5 and 14MeV neutrons have similar shape.

ACKNOWLEDGEMENTS

We would like to acknowledge the support and contributions of the JET team listed in [1].

REFERENCES

[1] The JET Team, Nucl. Fusion **32** (1992) 187.

[2] JARVIS, O.N., Rev. Sci. Instr. **63** (1992) 4511.

[3] ADAMS, J.M., CHEETHAM, A., CONROY, S., et al., in Controlled Fusion and Plasma Physics (Proc. 16th Europ. Conf., Venice, 1989), Vol. 1, European Physical Society (1989) 63.

[4] ADAMS, J.M., JARVIS, O.N., SADLER, G., et al., The JET Neutron Emission Profile Monitor, JET preprint JET-P(92)27 (1992), to be published in Nucl. Instr. Meth.

[5] JARVIS, O.N., Neutron and Gamma Ray Diagnostics, Parts I. and II., in International School of Plasma Physics - "Piero Caldirola", Diagnostics for Contemporary Fusion Experiments, P.E. Stott, D.K. Akulina, G. Gorini and E. Sindoni (Eds.), SIF, Bologna 1991, p. 541.

[6] JARVIS, O.N., CLIPSHAM, E.W., HONE, M.A., et al., Fusion Technology **20** (1991) 265.

[7] MARCUS, F.B., ADAMS, J.M., CHEETHAM, A.D., et al., Plasma Physics and Controlled Fusion **33** (1991) 277.

[8] GRANETZ, R.S., SMEULDERS, P., Nucl. Fusion **28** (1988) 457.

[9] CONROY, S.W., Diagnosis of Fusion Products for Reactor Relevant Plasmas, Ph.D Thesis, Imperial College, London (1990).

[10] JARVIS, O.N., ADAMS, J.M., CONROY, S., et al., in Controlled Fusion and Plasma Physics (Proc. 18th Europ. Conf., Berlin, 1991), Vol. 1, European Physical Society (1991) 21.

[11] SADLER, G., CONROY, S., JARVIS, O.N., van BELLE, P., ADAMS, J.M., and HONE, M., Fusion Technology **18** (1990) 556.

[12] CONROY, S.W., ADAMS, J.M., BOND, D.S., et al., Bull. Am. Phys. Soc. **36** (1991) 2367.

[13] GOLDSTON, R.J., McCUNE, D.C., TOWNER, H.H., et al., J. Comput. Phys. **43** (1981) 61.

[14] BALET, B., STUBBERFIELD, P.M., BORBA, D., et al., "Particle and Energy Transport During the First Tritium Experiments on JET," Nucl. Fusion, accompanying paper in this issue.

[15] SMEULDERS, P., ADAMS, J.M., BALET, B., et al., in Controlled Fusion and Plasma Physics (Proc. 17th Europ. Conf., Amseterdam, 1990), Vol. 1, European Physical Society (1990) 323.

[16] STORK, D., ALPER, B., ALI-ARSHAD, S., et al., in Controlled Fusion and Plasma Physics (Proc. 19th Europ. Conf., Innsbruck, 1992), Vol. 1, European Physical Society (1992) 339.

[17] BEHRINGER, K., et al., Proc. 11th IAEA Conf. on Plasma Phys. and Contr. Fusion Research, 1986, **1** (1987) 197.

[18] GONDHALEKAR, A., CHEETHAM, A.D., de HAAS, J.C.M., et al., Plasma Physics and Controlled Fusion **31** (1989) 805).

[19] HORTON, L.D., ANDREW, P., BRACCO, G., et al., Proc. of the 10th Int. Conf. on Plasma Surface Interactions (1992) Monterey, CA, USA.

[20] ADAMS, J.M., BALET, B., BOYD, D.A., et al.,

[21] SPITZER, L., Physics of Fully Ionized Gases, 2nd edn. Interscience, New York, 1962.

[22] JARMIE, N., BROWN, R.E., and HARDEKOPF, R.A., Phys. Rev. C, **29** (1984) 2031.

[23] CORE, W.G.F., van BELLE, P., and SADLER, G., in Controlled Fusion and Plasma Physics (Proc. 14th Europ. Conf., Madrid, 1987), Vol. IID, European Physical Society (1987), Part I, p. 49.

[24] JARVIS, O.N., ADAMS, J.M., BALET, B., et al., Nucl. Fusion **30** (1990) 307.

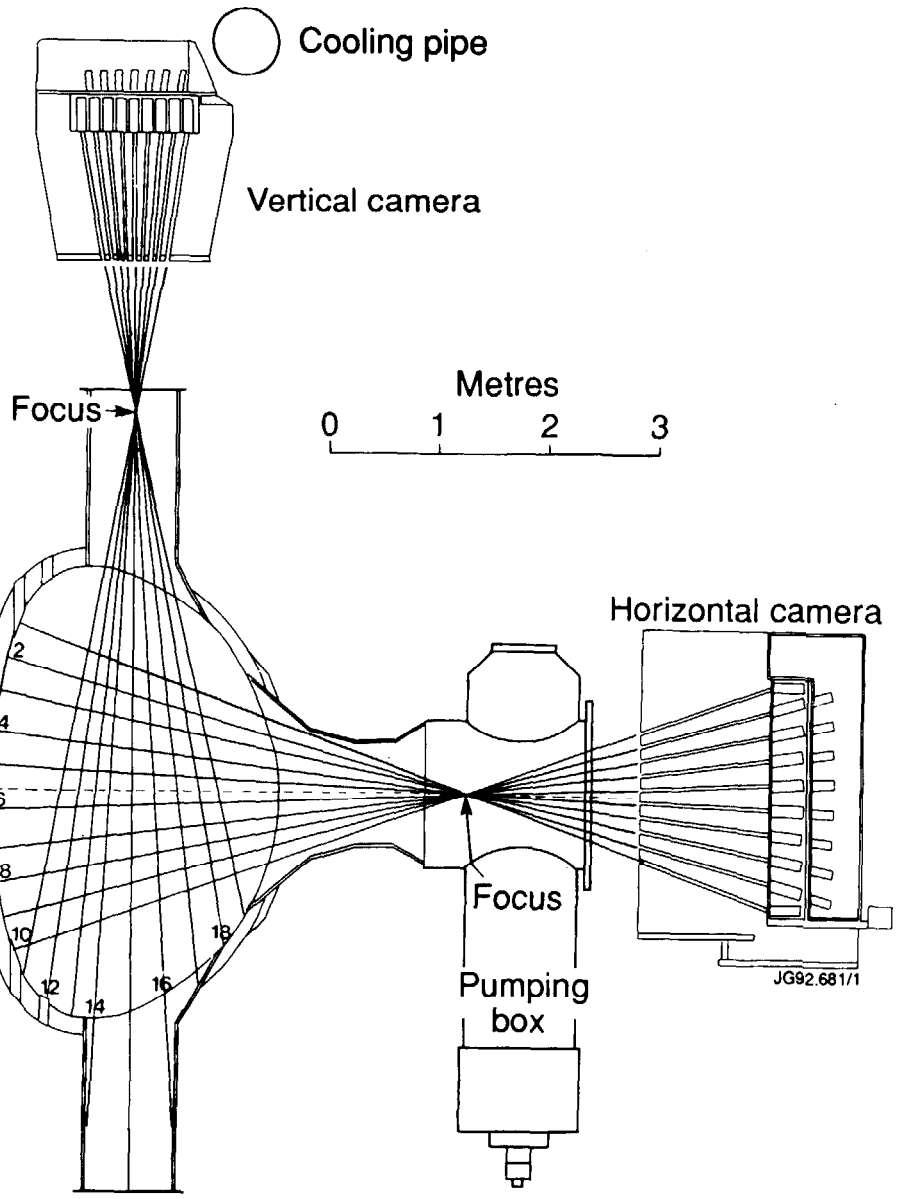

Fig.1 The Jet neutron emission profile monitor [3,4] is drawn schematically, showing the lines-of-sight. It consists of two fan-shaped multi-collimator cameras using NE-213 scintillators.

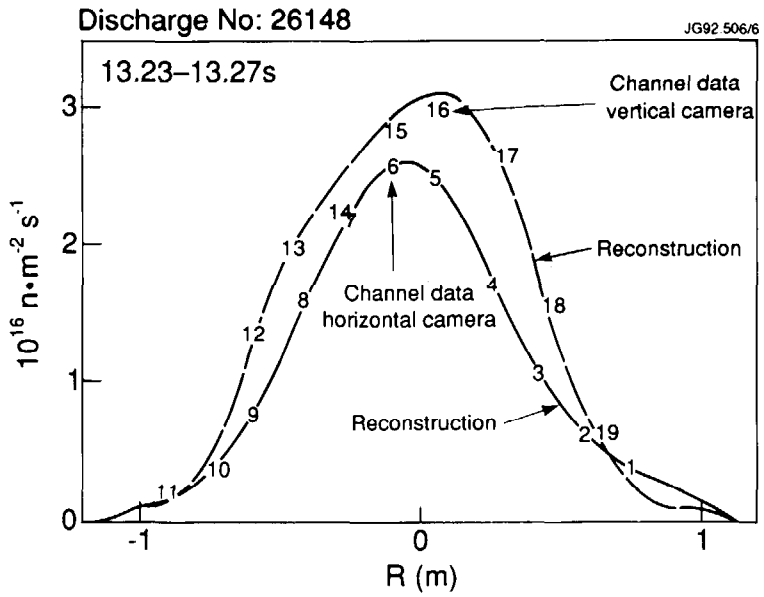

Fig.2 A comparison is made between measured line-integrals and those calculated from tomographic reconstruction. The measured line-integrals for each channel of the two neutron cameras are plotted as numbers, and calculated line-integrals are displayed by the solid and dashed curves for the horizontal and vertical cameras respectively. The abscissa gives the radius in the median plane of the ellipse tangent to each channel. The data were time-integrated from 13.23s to 13.27s for Discharge No: 26148.

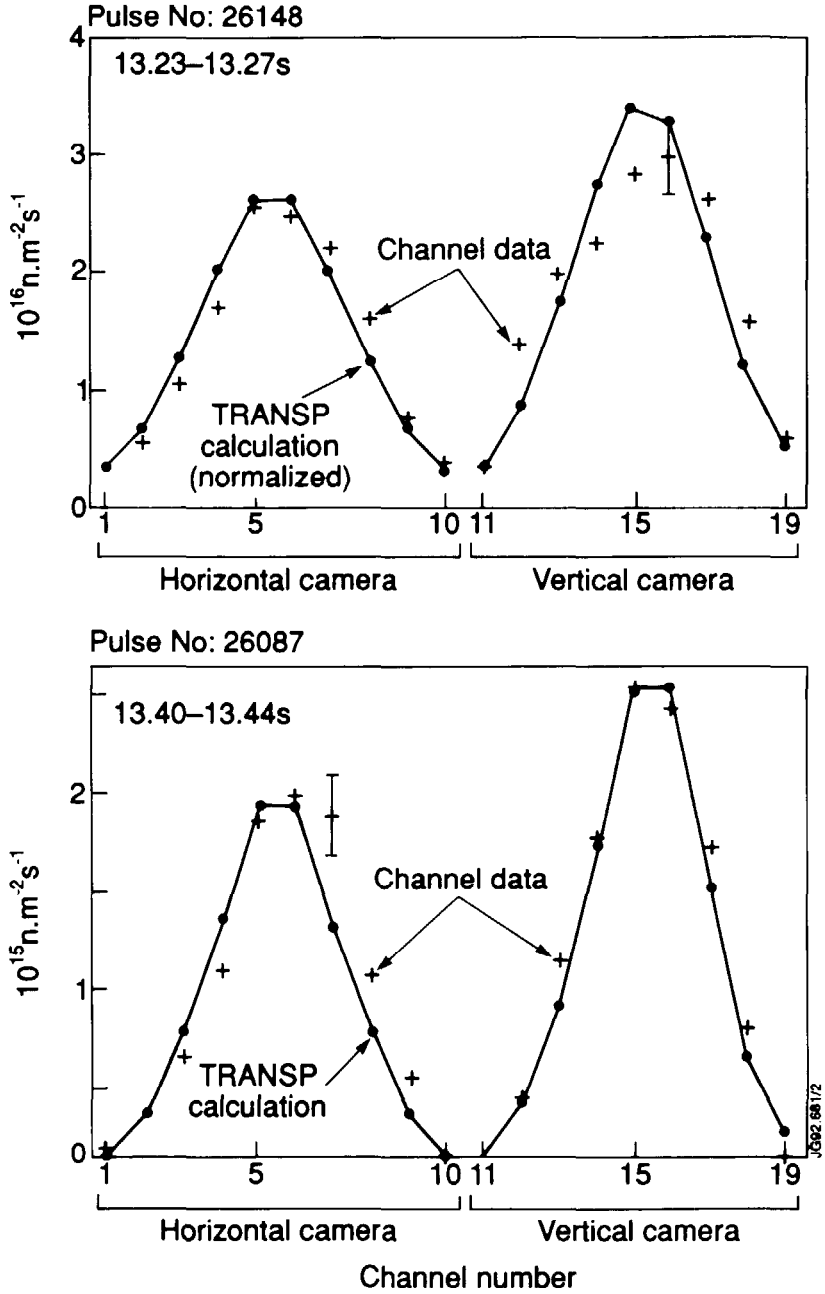

Fig.3 The normalized neutron fluxes (with error bars) are compared with normalized line-integral emissions calculated for each neutron camera channel from a TRANSP simulation for (a) 14MeV neutrons from Discharge No: 26148 and (b) 2.5MeV neutrons from Discharge No: 26087.

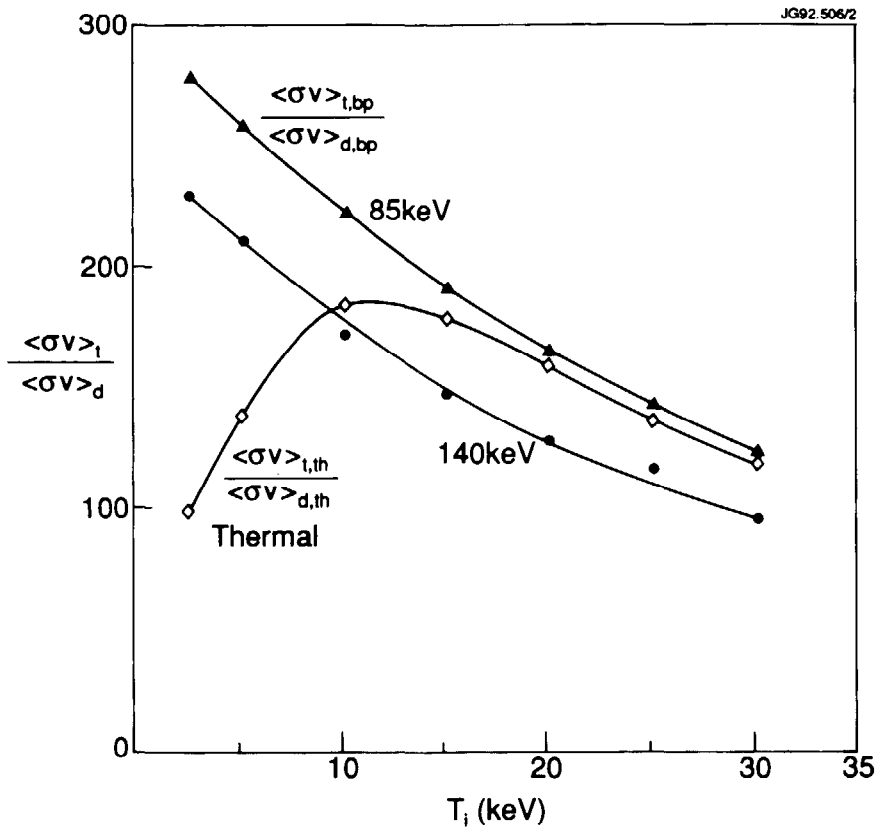

Fig.4 The ratio of thermal deuterium–tritium to thermal deuterium–deuterium ($\langle\sigma v\rangle$th) reactivities, and the ratios of deuterium beam–tritium plasma to deuterium beam–deuterium plasma ($\langle\sigma v\rangle_{bp}$) reactivities, for deuterium beam energies of 140keV and 85keV, typical of the JET PINIs, are plotted versus plasma ion temperature T_i.

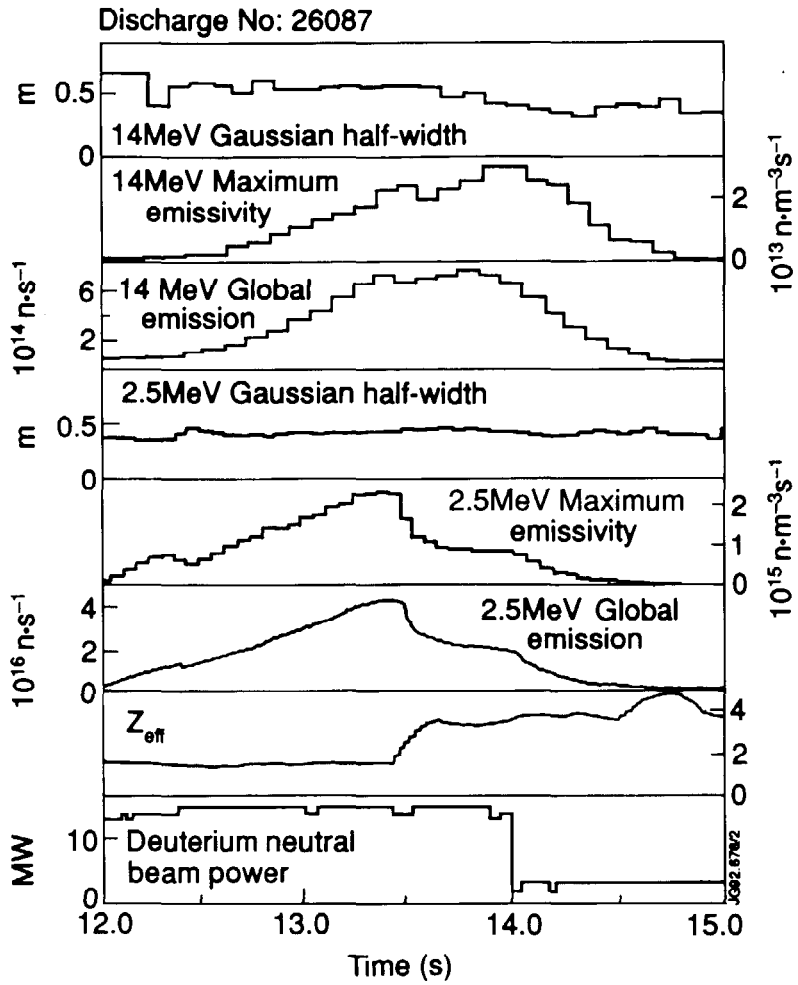

Fig.5 The 2.5 and 14MeV neutron gaussian half-widths, maximum emissivities and global emissions, plasma effective charge Z_{eff}, and the deuterium neutral beam power are displayed versus time for Discharge No: 26087.

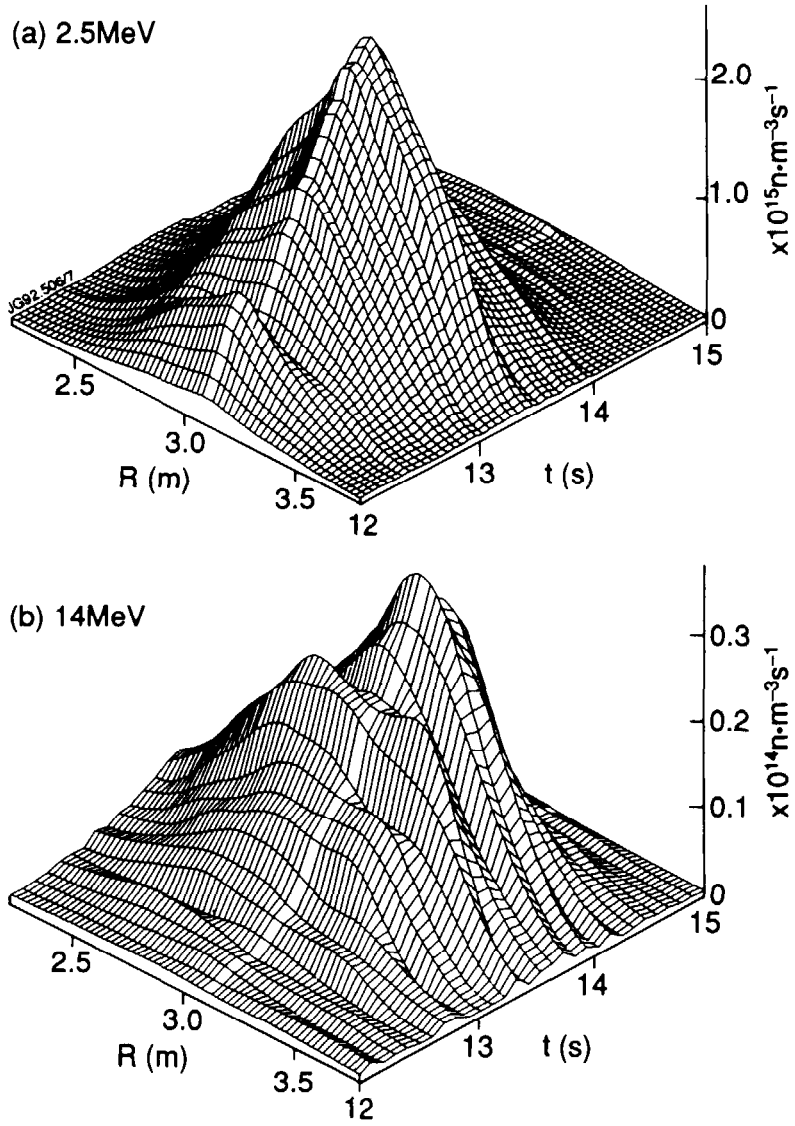

Fig.6 1-D cuts of the (a) 2.5MeV and (b) 14MeV neutron 2-D emissivity profiles are plotted as functions of time and radius along a major radius chord through the plasma midplane (z=0) for discharge No: 26087 during and after high power neutral beam heating.

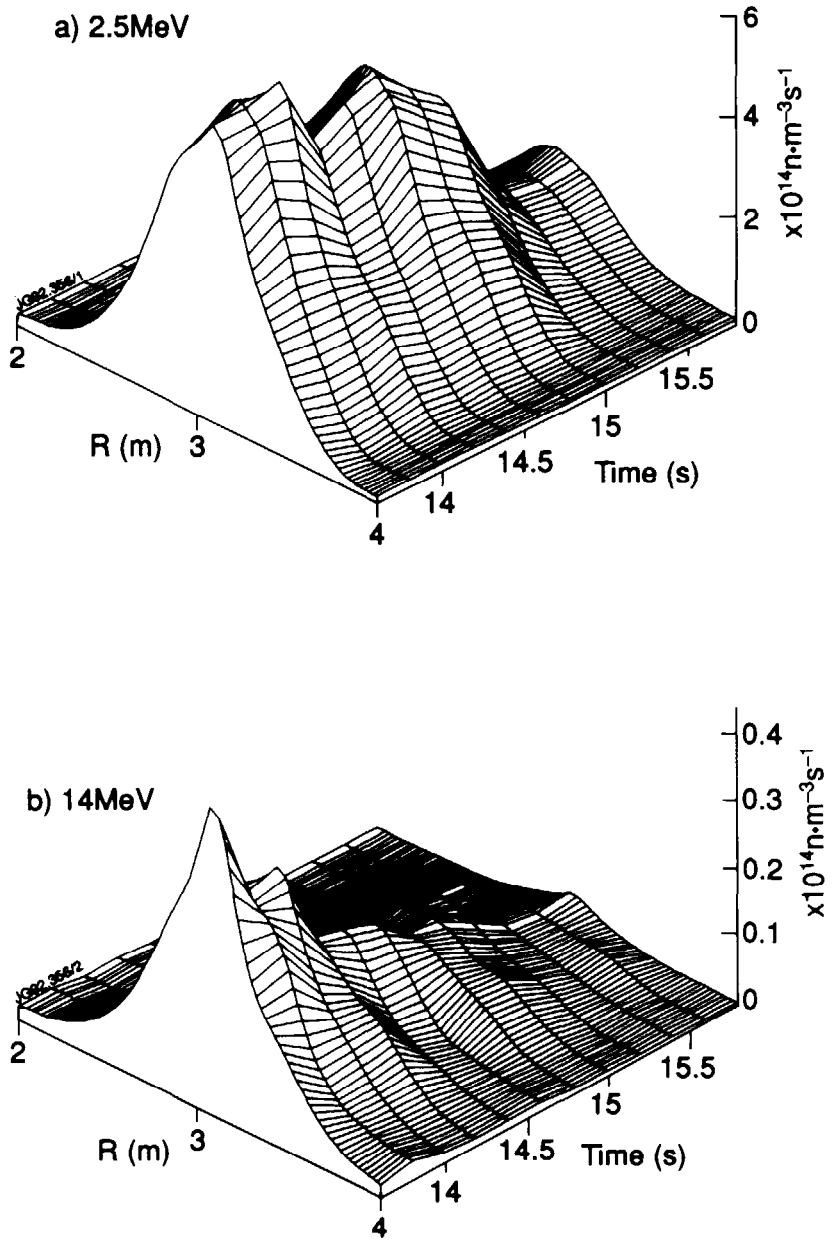

Fig.7 neutron emissivity profiles along a radial chord at the tokamak midplane are plotted versus major radius and time for the (a) 2.5MeV, and (b) 14MeV neutrons from discharge No: 26114.

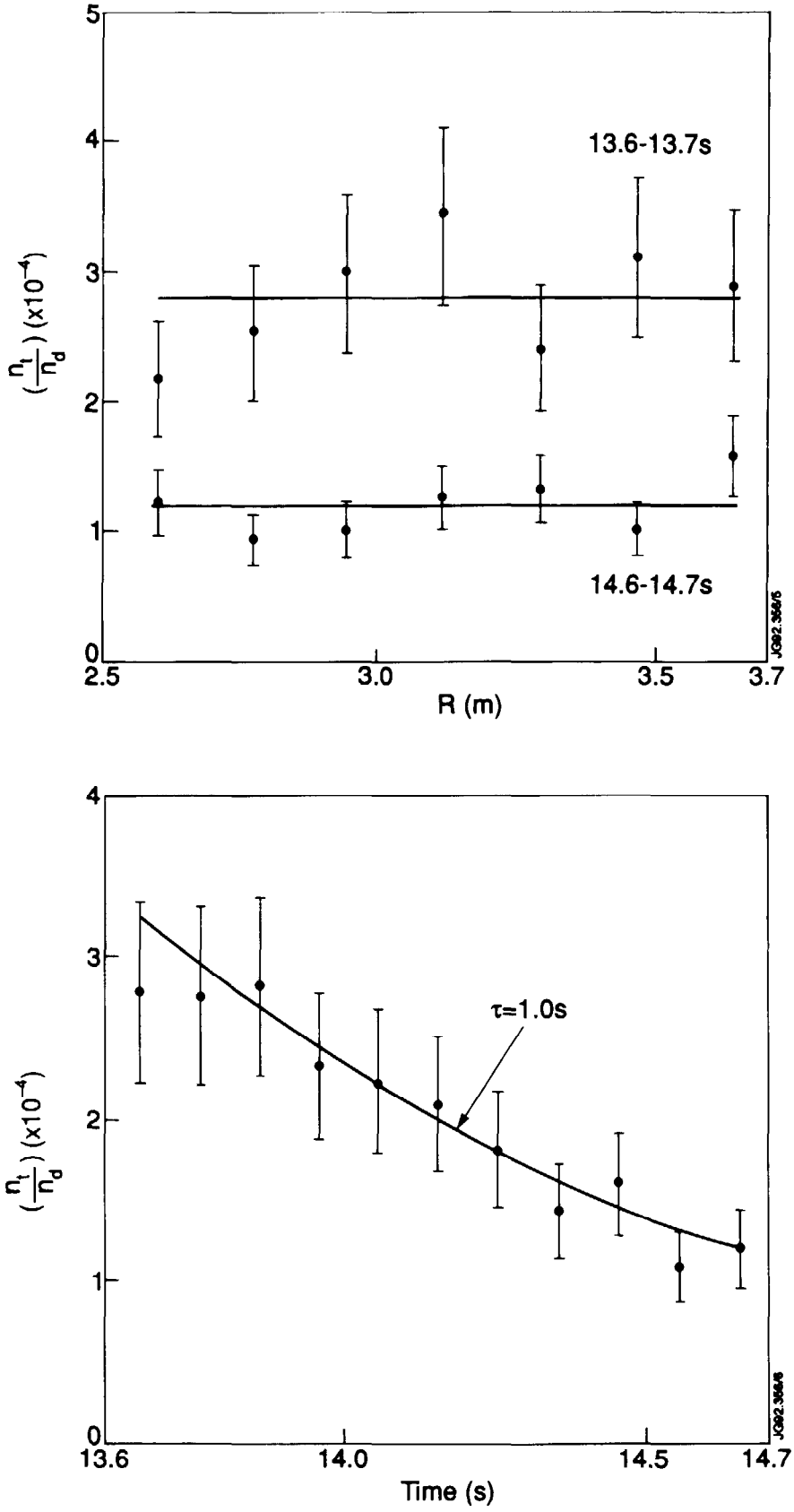

Fig.8 (a) The ratio n_t/n_d and its radially-averaged value are plotted versus major radius for two different time points during the tritium density decay phase of discharge No: 26114. (b) The radially-averaged density ratio n_t/n_d is plotted as a function of time. The fitted exponential curve has a 1.0s decay.

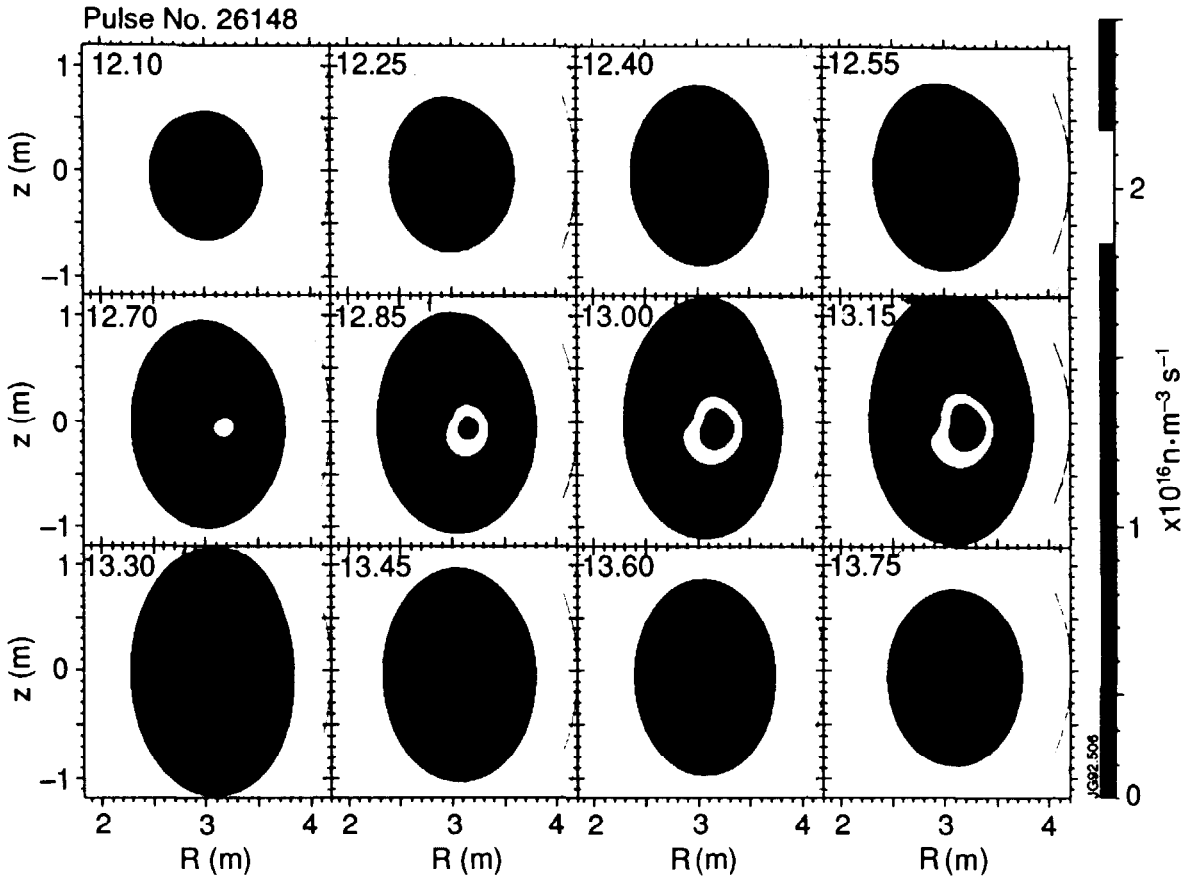

Fig.9 Tomographic inversion of the data was performed to obtain the 2-D neutron emissivity profiles presented as colour contour plots. The 14MeV neutron emissivity is plotted versus major radius and vertical height at 150ms intervals, covering the high power heating phase for discharge No: 26148.

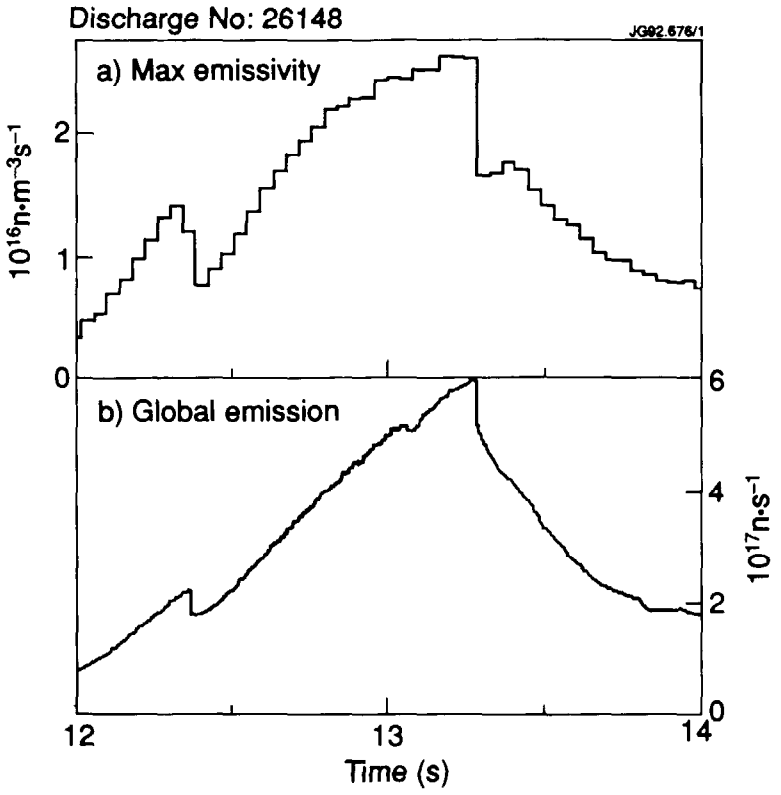

Fig.10 Time traces are shown of (a) the maximum local emissivity, (b) the global 14MeV neutron emission, during the high power heating phase of discharge No: 26148 from 12s to 14s.

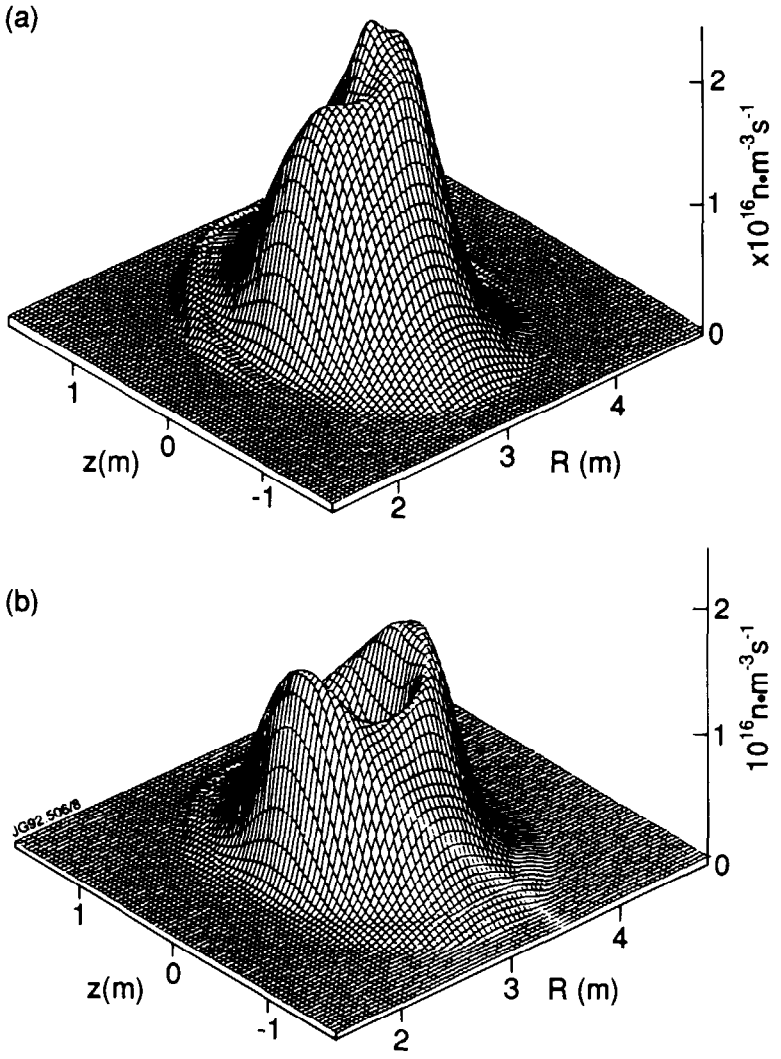

Fig.11 The 2-D emissivity profiles of the 14MeV neutrons are displayed versus major radius R and height z for 2.5ms time bins, (a) at 13.28s, just before the sawtooth crash, and (b) at 13.29s, just after the crash, in discharge No: 26148.

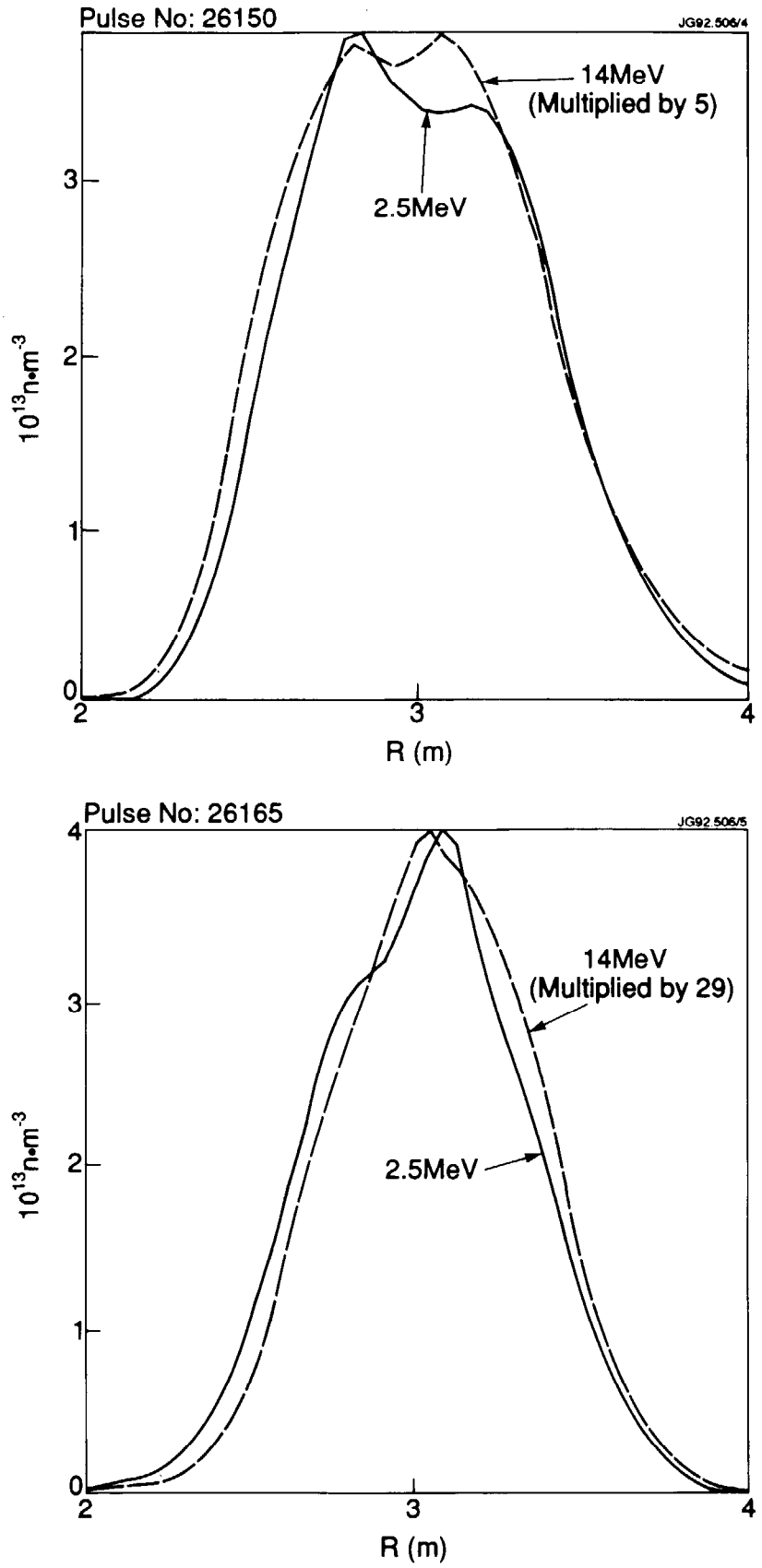

Fig.12 The 2.5MeV and (scaled up) 14MeV neutron emissivities are plotted along the major radius chord through the magnetic axis for (a) No: 26150 and (b) No: 26165 during the tritium cleanup experiments.

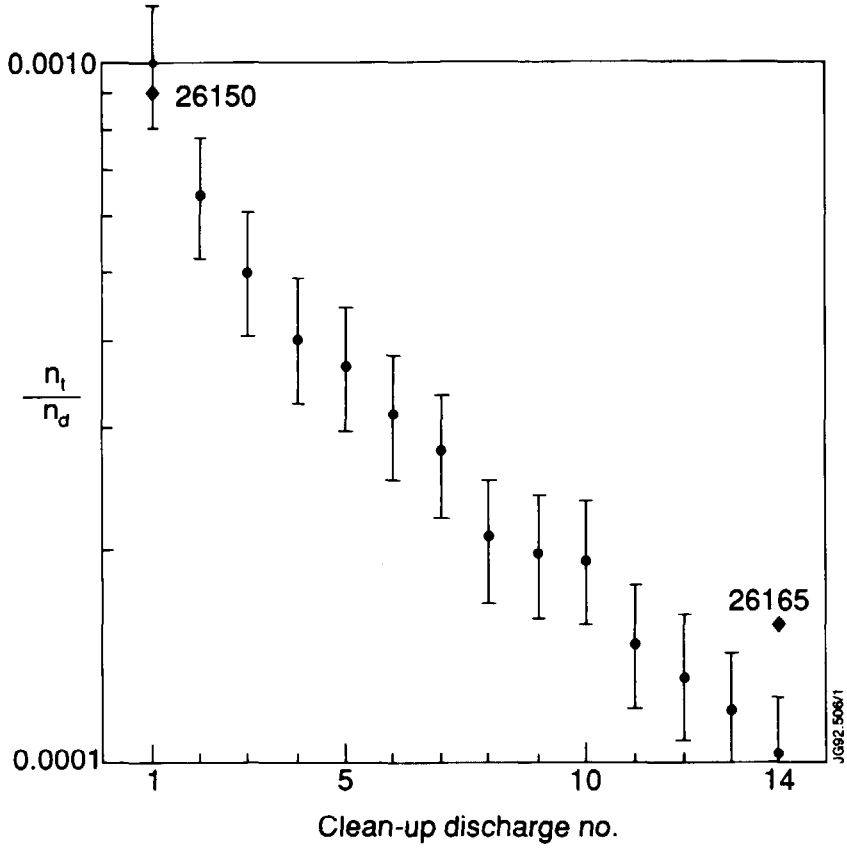

Fig.13 The density ratio n_t/n_d derived from global neutron emission rates (dots with error bars) integrated from 8.5 to 9.0s, and local emissivity integrated from 8-18s (diamonds) is plotted as a function of discharge number for No: 26165 during the tritium cleanup experiments.